A&A 543, A101 (2012)
DOI: 10.1051/0004-6361/201219022
© ESO 2012

Astronomy & Astrophysics

New members of the massive stellar population in Cygnus★,★★,★★★

F. Comerón[1] and A. Pasquali[2]

[1] ESO, Karl-Schwarzschild-Strasse 2, 85748 Garching bei München, Germany
e-mail: fcomeron@eso.org
[2] Astronomisches Rechen-Institut, Zentrum für Astronomie der Universität Heidelberg, Mönchhofstr 12–14, 69120 Heidelberg, Germany
e-mail: pasquali@ari.uni-heidelberg.de

Received 12 February 2012 / Accepted 17 April 2012

ABSTRACT

Context. The Cygnus OB2 association and its surroundings display the richest collection of massive stars in our nearby Galactic environment and a wealth of signposts of the interaction between these stars and the interstellar gas.
Aims. We perform a magnitude-limited, homogeneous census of O and early B-type stars with accurate spectral classifications in the blue, in a $6° \times 4°$ region centered on Cygnus OB2 that includes most of the Cygnus X complex, a sizeable fraction of the adjacent Cygnus OB9 association, and a large area of the field surrounding these complexes.
Methods. By using reddening-free indices based on $BJHK$ magnitudes from the USNO-B and 2MASS catalogs, we are able to produce a highly complete, highly uncontaminated sample of O and early B stars, which nearly duplicates any previous census of the region for the same range of spectral types. We provide the spectral types of 60 new O and B stars, as well as a list of an additional 60 candidates pending spectroscopic confirmation. In addition, the UBV imaging of the surroundings of three apparently isolated O stars is used to investigate the possible presence of small clusters of young stars around them.
Results. Early-type stars are consistent with similar distances for Cygnus OB2, OB9, and the field stars surrounding them. We confirm previous findings of an older population in Cygnus OB2 spatially offset from where the stellar density of the association peaks. Some new remarkable objects are identified, including BD+40 4210, a B0 supergiant member of Cygnus OB2 that is among the brightest members of the association sharing some characteristics with luminous blue variable (LBV) candidates, located at a projected distance of 5 pc from another LBV candidate. A new O5If member of Cygnus OB9 is found, as well as several other O stars and B supergiants. On the other hand, while no obvious clustering is found around the apparently isolated O stars, the fields around two of them seem to contain objects with strong ultraviolet excesses, which perhaps indicates that they are accreting, although their nature and possible relationship to the O stars in the field are unclear.
Conclusions. Star formation in Cygnus has been taking place in a sustained manner for well over 10 Myr, with a large-scale trend of proceeding from lower to higher Galactic longitudes. Star formation inside Cygnus OB2 follows this trend, with indications of intense star formation activity having started in the southern (lower galactic latitude) part of the association about 10 Myr ago and probably continuing at present in the north.

Key words. stars: early-type – stars: formation – open clusters and associations: individual: Cygnus OB2 – open clusters and associations: individual: Cygnus OB9 – ISM: individual objects: Cygnus X

1. Introduction

The massive-star forming complexes in Cygnus (Reipurth & Schneider 2008) are among the most well-suited regions of our Galactic neighborhood to study the processes leading to the formation of large stellar complexes along spiral arms (Elmegreen 2004) and the interaction between massive stars and the interstellar medium. The region is extraordinarily rich in signposts of massive star formation, both recent and ongoing (e.g. Odenwald & Schwartz 1993). It contains several OB associations (Humphreys 1978; Garmany & Stencel 1992; Mel'nik & Efremov 1995; Knödlseder et al. 2002), including the very rich Cygnus OB2 association, and abundant molecular and ionized gas mainly in the large Cygnus X complex (Wendker et al. 1991; Schneider et al. 2006). It has also been found that related to these complexes are large-scale structures such as HI bubbles and the still enigmatic Cygnus superbubble (Cash et al. 1980; Bochkarev & Sitnik 1985; Uyaniker et al. 2001) that may have been produced by the combined energetic activity of the massive stars in the region (Comerón et al. 1998). The region is also a unique high-energy laboratory providing direct insight into the nucleosynthesis processes taking place in massive stars (Knödlseder et al. 2002; Martin et al. 2010).

The Cygnus star-forming complexes extend over a wide interval in Galactic longitude (roughly $70° < l < 95°$) and most probably also in distance. Some prominent complexes in this region of the sky, such as the Cygnus OB7 association and the North America and Pelican nebulae, are most likely less than 1 kpc from the Sun (Garmany & Stencel 1992; Laugalys & Straizys 2002; Comerón & Pasquali 2005), while the kinematics of other objects in the same general direction clearly associate them with the more distant Perseus arm in the background. However, the bulk of massive-star formation in Cygnus

★ Based on observations collected at the Centro Astronómico Hispano-Alemán (CAHA) at Calar Alto, operated jointly by the Max-Planck Institut für Astronomie and the Instituto de Astrofísica de Andalucía (CSIC); and with the IAC80 telescope operated on the island of Tenerife by the Instituto de Astrofísica de Canarias in the Spanish Observatorio del Teide.
★★ Tables 1–7 are available at http://www.aanda.org
★★★ Tables 1–7 are also available at the CDS via anonymous ftp to cdsarc.u-strasbg.fr (130.79.128.5) or via http://cdsarc.u-strasbg.fr/viz-bin/qcat?J/A+A/543/A101

appears to lie at roughly 1.4–1.5 kpc from the Sun (Knödlseder 2002; Rygl et al. 2011). At these distances, the complex is dominated by the very rich and compact association Cygnus OB2 (Torres-Dodgen 1991; Knödlseder 2000, 2003; Comerón et al. 2002), other neighboring associations such as Cygnus OB9, and the massive-star forming complex Cygnus X, all testifying to the vigorous, extended star-forming activity occurring at present in this area (Schneider et al. 2006; Reipurth & Schneider 2008). However, evidence has been found in recent years of massive-star formation extending into the past and perhaps predating the birth of Cygnus OB2. In her spectroscopy study of new candidate O and B stars in Cygnus OB2 identified by Comerón et al. (2002), Hanson (2003) found a large number of B stars of luminosity classes I to III, which she interpreted as an older, more spatially distributed population. A similar result was found by Comerón et al. (2008), who showed that the population of evolved stars with massive progenitors ($M > 10\ M_{\odot}$) extends beyond the boundaries of Cygnus OB2 and most likely beyond a 2° radius around the association (see also Drew et al. 2008; Wright et al. 2010). These evolved B stars represent a previous generation of massive stars that sculpted the local interstellar medium, out of which the present generation formed, and were perhaps responsible for the formation of large-scale structures such as the Cygnus superbubble.

In this paper, we study the massive star content of a large area extending 6° × 4° in Galactic longitude and latitude, respectively, centered on Cygnus OB2. It includes much of the neighboring association Cygnus OB9, as well as the Cygnus X complex and several other star-forming regions. The massive stellar component of some of these regions has been the subject of previous studies, most notably Cygnus OB2 itself (Massey & Thompson 1991; Hanson 2003; Comerón et al. 2002, 2008; Kiminki et al. 2007; Negueruela et al. 2008), and the open cluster NGC 6910, which possibly belongs to Cygnus OB9 (Delgado & Alfaro 2000). However, no homogeneous study with a uniform selection criterion for the identification of massive stars over the entire area has been carried out in the recent past. In the present study, we use the combined visible and near-infrared photometry provided by the United States Naval Observatory-B (USNO-B) and Two-Micron All-Sky Survey (2MASS) catalogs to produce a large list of candidate O and B stars in the area. Many of them have already been identified and spectroscopically classified in previous studies, but we increase the census by adding 60 new O and B stars, for which spectral types are provided. We also produce a list of additional candidate O and B stars for future spectroscopic classification that, if confirmed, and together with the new stars already classified in the present work, will double the census of O and B stars in this region of Cygnus. The results allow us to explore systematic trends in age and to produce a more complete assessment of the massive stellar content of the region. Some of the newly identified stars are found to have O types but they do not seem to belong to any of the previously known clusters or associations. We present here *UBV* imaging designed to detect unknown star clusters or aggregates in the vicinity of four of them.

2. Target selection

The power of near-infrared (NIR) observations in revealing the true structure, content, and extension of Cygnus OB2 and its surroundings was dramatically demonstrated by Knödlseder (2000), who used star counts in the 2MASS Point Source Catalog (Skrutskie et al. 2006) to suggest that Cygnus OB2 is comparable in both richness and extent to a young globular cluster. Comerón et al. (2002) used 2MASS-based color–color criteria to select a sample of candidate O and B stars for which they obtained *H*- and *K*-band low-resolution spectroscopy. These NIR spectra confirmed that most of the photometrically selected objects were indeed early-type stars, some of them displaying emission lines typical of evolved stages (Morris et al. 1996). Accurate spectral types in the visible of the least obscured early-type candidates of Comerón et al. (2002) were obtained by Hanson (2003), who confirmed them to be O and B stars with types B2 or earlier. The success rate of the near-infrared color criterion was further exploited by Comerón et al. (2008) to identify additional early-type stars in the surroundings of Cygnus OB2. The spectroscopic follow-up of that work shows that about half of the sample selected based on 2MASS colors is actually composed of late-type stars, including long-period variables and carbon stars.

The combination of CCD photometry in the visible from the USNO-B catalog with near-infrared photometry from 2MASS in the NOMAD catalog (Zacharias et al. 2004) and more recently in the UCAC3 catalog (Zacharias et al. 2010) allowed us to refine our earlier photometric selection criteria. The inclusion of a data point at visible wavelengths in order to more tightly constrain the intrinsic spectral energy distribution of stars proves to be very helpful in distinguishing between reddened early-type stars and intrinsically red late-type stars. After experimenting with reddening-free indices based on the *B*, *R*, *I*, *J*, *H*, and *K* bands, we find that the index cuts

$$Q_{BJK} = 0.196(B-J) - 0.981(J-K) - 0.098 > 0 \quad (1)$$

$$Q_{JHK} = 0.447(J-H) - 0.894(H-K) - 0.089 < 0 \quad (2)$$

are most efficient in discarding late-type contaminants when applied to the spectroscopically observed samples of Comerón et al. (2002, 2008). The coefficients multiplying the various colors are empirically determined by plotting the stars in the region on the $(B-J)$, $(J-K)$ and the $(J-H)$, $(H-K)$ diagrams respectively, thus tracing the direction of the extinction vector. Most of the values obtained are within 10% of those derived using the Rieke & Lebofsky (1985) extinction law for the diffuse interstellar medium. The exception is the coefficient multiplying the $(B-J)$ color, which is 22% higher than the corresponding Rieke & Rieke (1985) value. This may be expected because of the greater tendency of shorter wavelengths to depart from the standard extinction law. The value that we empirically determine is actually close to that obtained from the Cardelli et al. (1989) extinction law for a total-to-selective extinction ratio $R_V = 4.0$, which is in-between the R_V values characteristic of the diffuse interstellar medium and of dense interstellar medium in star-forming regions. Evidence of a high value of R_V in the direction of Cygnus was presented by Terranegra et al. (1994), which agrees with our finding.

We thus used the *BJHK* photometry tabulated in the NOMAD catalog[1] to obtain a large sample of candidate O and B stars in the 6° × 4° area limited in Galactic coordinates by $77°5 < l < 83°5$, $-1°2 < b < 2°8$. We set a near-infrared limiting magnitude of $K_S = 9.0$ to reduce the number of early-type stars background to the Cygnus complex. The limit corresponds to $M_K \simeq -2.3$ at the estimated distance of Cygnus OB2, assuming a foreground extinction of $A_V \simeq 5$ as typically found among

[1] The more recent UCAC3 catalog (Zacharias et al. 2010) also provides this merged information. However, UCAC3 not having yet been published at the time when we carried out our sample selection, we preferred to keep the reference to the NOMAD catalog for consistency.

the stars of that association (e.g. Massey & Thompson 1991; see also Sect. 4). Furthermore, to produce a sample that can be spectroscopically confirmed in the B band with a 2m-class telescope and a reasonable investment of observing time, we retained only stars with $B < 16$. The combination of the K_S and B magnitude cuts with the intrinsic $(B-K)$ colors of O and B stars implies that our selection criteria are sensitive to any main-sequence stars earlier than B1 and obscured by $A_V < 6.7$ mag, as well as to stars brighter in K and even more obscured. We note that the selection criterion $Q_{BJK} > 0$ also discriminates against objects having substantial K-band excess, as commonly found among B[e] stars (Kastner et al. 2010).

A literature search reveals that many of the stars in our sample have already been spectroscopically classified by previous surveys, as our selection criteria recover most of the known O and B stars in Cygnus OB2 and Cygnus OB9. However, about half of the sample is composed of stars not previously recognized as early-type, or by stars whose early-type nature had only been roughly established by low-dispersion objective prism spectroscopy. In a small number of cases, published spectral types or those determined by us show that the stars are actually later than B, showing that the new selection criterion is not entirely free from contamination. Nevertheless, its derived success rate of ~80% (defined as the ratio of the spectroscopically confirmed O and B stars to candidates selected by means of the photometric criterion) proves it to be very efficient for our purposes.

The $B - K_S, K_S$ diagram of the stars selected by our criteria (1) and (2) is presented in Fig. 1. Their distribution shows that most of them have magnitudes and colors characteristic of moderately reddened O and early B stars at the distances commonly estimated for the OB associations in the area. We note, however, the presence of stars with very bright K_S magnitudes, having colors well within the range of those of fainter stars in the region. Spectral classifications are available for almost all of them, showing that they are actual O and B stars rather than foreground later-type stars contaminating the sample. Furthermore, that our Q_{BJK} criterion excludes stars with strong infrared excesses as noted above indicates that these stars have very high intrinsic luminosities, as confirmed by their spectroscopic classification as blue supergiants (Sect. 3.1).

While most of the stars in the region lie within the boundaries of Cygnus OB2 or Cygnus OB9, some are rather distant from these associations as well as from any other known cluster. We thus selected three of these apparently isolated, spectroscopically confirmed O stars for follow-up imaging observations, in order to search for possible still unknown clusters in their surroundings and thus check whether they are truly isolated.

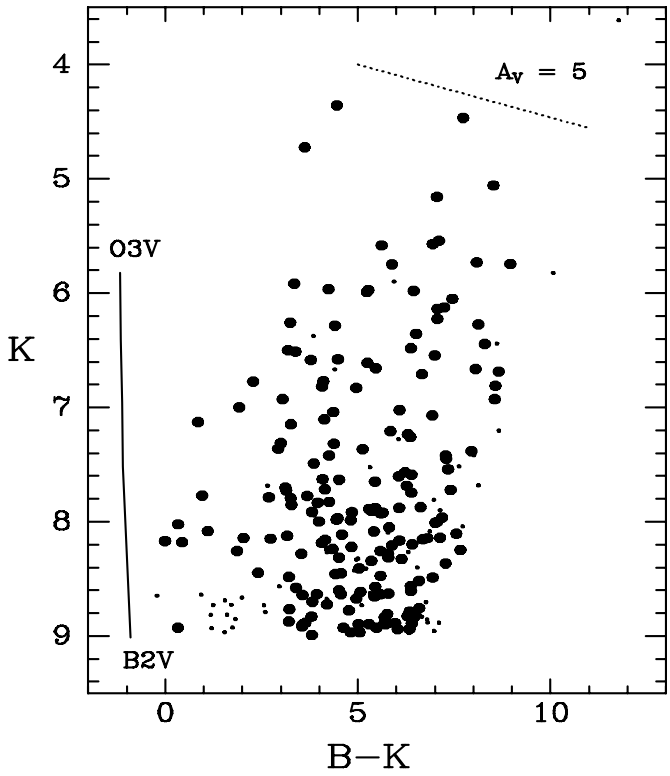

Fig. 1. Color–magnitude diagram of stars selected using the criteria given by Eqs. (1) and (2). Stars retrieved by those criteria but with confirmed later spectral types (see Sect. 3.1) have been excluded. Filled circles are O and B-type stars spectroscopically confirmed, either by previous studies or by the present one, and dots are O and B-type candidates lacking spectroscopic confirmation. The solid line marks the position of the unreddened upper main sequence based on the "observational" $T_{\rm eff}$ scale of Martins et al. (2006) shifted to a distance modulus $DM = 10.8$. The dotted line represents the displacement caused in the diagram by an extinction of $A_V = 5$ mag, using the reddening law of Cardelli et al. (1989) with total-to-selective extinction ratio $R_V = 3.1$. The sharp cuts in the distribution of points are due to our magnitude limits $K_S < 9$, $B < 16$.

3. Observations

3.1. Spectroscopy and spectral classification

Spectroscopy in the visible of more than half (see Sect. 4) of the new O and B candidate stars that were photometrically selected was obtained with the 2.2 m telescope of the Calar Alto observatory using CAFOS, the facility visible-light imager and low-resolution spectrograph, during three observing runs in July 2006, July–August 2008, and July–August 2010, the last two being conducted in service mode by the observatory. The grism used covered the range shortwards of $\lambda = 6350$ Å at a resolution of $\lambda/\Delta\lambda = 1000$ with a 1.″5 slit. Exposure times were decided based on the B magnitude, and ranged from 10 min for the brightest sources to 180 min for the faintest. For integration times longer than 30 min, the exposures were divided into blocks of 30 min. Spectra of three lamps of HgCd, He, and Rb were taken between subsequent exposures for wavelength calibration, to minimize the effects of instrument flexure. The frames containing the raw spectra were corrected for the effects of both bias and flat field, and the spectra were subsequently extracted from each one of them. The individual wavelength-calibrated spectra were coadded after identification and removal of cosmic ray hits. The coadded spectra were finally normalized to the interpolated continuum.

The extracted spectra were classified using as a reference the extensive atlas of early spectral types of Walborn & Kirkpatrick (1990), which is well-suited to our work given its spectral resolution similar to that of our observations and its dense grid of O and B spectral types with different luminosity classes. We used the spectral subtype and luminosity class indicators noted in the atlas, which were summarized in Comerón et al. (2008) for the range of interest in this work. All the early-type stars in our sample are significantly obscured and display prominent interstellar absorption features, particularly the diffuse interstellar bands. Approximate uncertainties in the spectral classifications were estimated to be one luminosity class and half a spectral subtype by comparing the independent classification of each spectrum by each of the authors. Some of the stars

observed by us also have spectral types published by other authors, particularly by Kiminki et al. (2007) and Negueruela et al. (2008), who carried out spectroscopic observations in the visible of photometrically selected stars from the studies of Massey & Thompson (1991) and Comerón et al. (2002), respectively. A comparison of our spectral classifications with those obtained by these authors generally confirms our estimate of the uncertainty, as discussed in Sect. 4.1.

3.2. Imaging

The UBV images of fields measuring $10\farcm1 \times 10\farcm1$ around three apparently isolated O stars newly classified by us were obtained with the CAMELOT camera at the IAC80 telescope at the Teide Observatory, on the nights of 1 to 4 September 2010. Four dithered observations of each field were performed in B and V with individual exposure times of 15 min and 8 min, respectively. For the U band, six observations of 30 min each were obtained. The images were bias-subtracted, flat-fielded and average-combined using standard IRAF[2] tasks. Point-spread function photometry was then performed using dedicated IRAF scripts making use of the DAOPHOT ALLSTAR task (Stetson 1987). Photometric calibration was carried out by obtaining a sequence of short exposures in a given filter of each of the four fields, with an observation of the open cluster NGC 6910 at the beginning and the end of the sequence. In this way, a set of local photometric standards was established for each field. The procedure was then repeated for the other two filters. The observations were carried out near the time of the meridian transit of the region. Photometric zeropoints and color terms were computed using the NGC 6910 stellar photometry published by Delgado & Alfaro (2000). We also made use of the average extinction coefficients publicly available for the Teide Observatory. The short photometric calibration exposures were also used to derive the magnitudes of the brightest stars in each field, which were saturated in the long exposures. The 5σ detection limits of our observations are $U = 22.1$ mag, $B = 23.4$ mag and $V = 22.4$ mag.

4. Results

The application of the selection criteria described in Sect. 2 to the sample of NOMAD stars within the area and B, K magnitude limits described there has provided us with a list of 260 photometrically selected stars. Of those, 119 are confirmed O- and B-type stars with spectral classifications available in the literature (Sect. 4.1). Of the remaining 141, we could confirm 60 as new O or early B stars. Another 20 stars selected by the criteria turn out to have A or later types, either already known from previous studies or revealed by our new spectroscopic observations. Finally, 61 photometrically selected stars remain unobserved spectroscopically and their possible early types are thus unconfirmed.

4.1. Known members

Most of the 119 of the O and B stars recovered by our selection criteria that had been previously classified as such in the region belong to Cygnus OB2. These stars are listed in Table 1, together with their published spectral types and the reference to the one that we adopt, since more than one spectroscopic classification is frequently found for the same star in the literature. Some of the stars listed in Table 1 were also observed by us, in most cases because they were included in the observing programs of other research teams while we were collecting data for the present study. The overlap of Table 1 with our own observations provides a useful benchmark for our own spectral classifications. The subset of stars of Table 1 for which we also obtained spectral types is listed in Table 2, where the comparison with the published spectral types confirms the estimated accuracy of our spectral classification as given in Sect. 3.1.

We compared our list of known members fulfilling (1) and (2) with that of Cygnus OB2 stars brighter than $B = 16$ and $K_S = 9$ spectroscopically classified as earlier than B2 by Massey & Thompson (1991). The comparison with a sample of confirmed O and early B stars independently selected should provide an accurate estimate of the degree of efficiency of our criterion, that is, the fraction of the actual population of O and B stars that are recovered by it. Of the 64 Cygnus OB2 stars that Massey & Thompson classify as earlier than B2, we found that 51 are brighter than our thresholds in B and K. Our selection criterion recovers 41 of those, leading us to estimate an efficiency of approximately 80% in selecting the O and B stars actually present in the region within the established magnitude limits[3]. The stars classified by Massey & Thompson (1991) as B2 or earlier that do not fulfill our selection criterion are listed in Table 6.

4.2. New O- and B-type stars

More than half of the candidate O and B stars identified by our selection criteria either have not been recognized as such in previous work, or have only rough spectral classifications published. We obtained classification quality spectra for 60 of them, listed in Table 3. Their spectra are displayed in Fig. 2. Table 4 list the remaining O and B candidates selected based on their $BJHK_S$ photometry for which we could not obtain photometry in the time allocated in the various observing runs. Given the high confirmation rate obtained for the spectroscopically confirmed stars, it is to be expected that approximately 80% of these stars also have O or B types.

The distributions in B magnitude of the known and newly identified O and B stars, including those pending spectroscopic confirmation among the latter, is presented in Fig. 3. The distributions are similar and show that the new members are slightly fainter, but insufficiently so to explain why they have been missed by previous surveys. Likewise, the distributions of derived visual extinction toward known members and spectroscopically classified new O and B stars are also shown in Fig. 3, showing that the new members are insignificantly more obscured on average than the known members.

Figure 4 shows the spatial distributions of the previously known O and B stars in the region together with the new, spectroscopically confirmed stars and the photometrically selected candidates for which no spectral classification is yet available. The majority of the newly confirmed members are located outside the region occupied by the brightest stars of Cygnus OB2, where most searches have been concentrated thus far. We do find new members of Cygnus OB2, as discussed in Sect. 5.1, but most of them are in a region adjacent to that containing the

[2] IRAF is distributed by NOAO, which is operated by the Association of Universities for Research in Astronomy, Inc., under contract to the National Science Foundation.

[3] Note that this is unrelated to the success rate previously quoted in Sect. 3, which also turns out to be around 80% and gives an indication of the reliability of the selection criteria in producing uncontaminated samples of O and B stars.

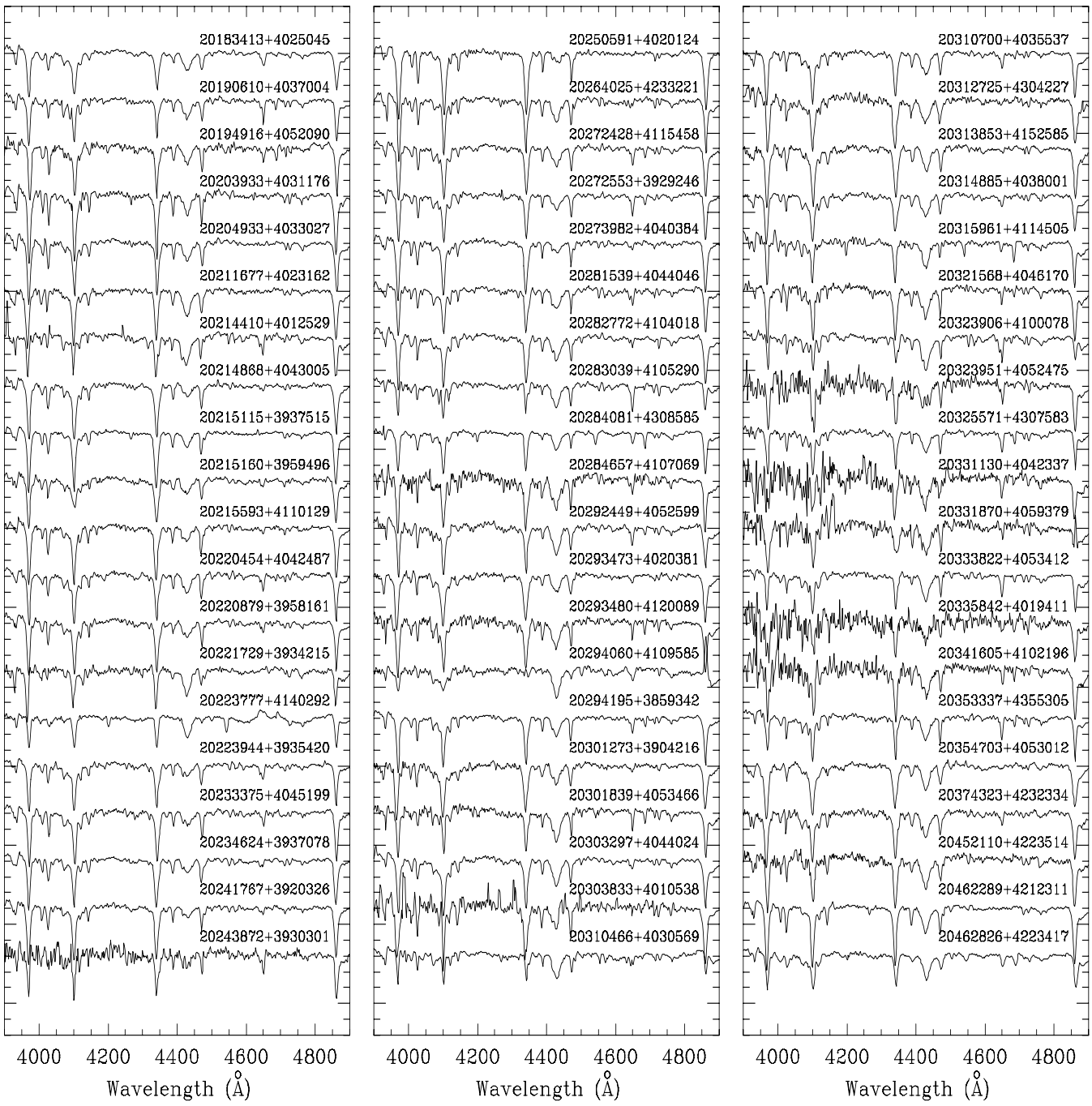

Fig. 2. Continuum-normalized spectra of all the stars listed in Table 3. For clarity, only the spectral region used for classification is shown.

largest number of its members. We also identify new members of Cygnus OB9, and many new O and B stars outside these two associations. It is thus apparent from Figs. 3 and 4 that the additions to the O and B census of the region provided by our work come from our having included in our survey, regions that had been either neglected by previous searches, or explored with far less detail than the most crowded regions of Cygnus OB2.

Our selection criteria identified 20 stars with types later than B based on previous spectral classifications, new spectral classifications obtained in this work, or existing photometry in other systems. These stars are listed in Table 5, where the variety of reasons that may contribute to their erroneous selection as candidate O or B stars can be appreciated. Their numbers relative to the stars listed in Tables 1 and 3 leads us to estimate a success rate of 80% of our criteria in the selection of true O and B stars.

4.3. Ages and initial masses

We used the 2MASS $(J - K_S)$ color and the intrinsic colors of both O stars from Martins & Plez (2006) and B stars from Tokunaga (2000), to estimate the foreground extinction toward each of the spectroscopically classified stars from Tables 1 and 3, using the extinction law of Cardelli et al. (1989). Temperatures were in turn assigned using the "observational" temperature scale of Martins et al. (2006) and the $T_{\rm eff}$ versus spectral type calibration of Tokunaga (2000). The procedure used is the same as that described in more detail in Comerón et al. (2008). Class V temperatures and colors were adopted in the cases for which no luminosity class could be determined. Given the typical estimated uncertainties of 0.5 subtypes in the spectral classification and 2 classes in the luminosity class, and that the uncertainty in

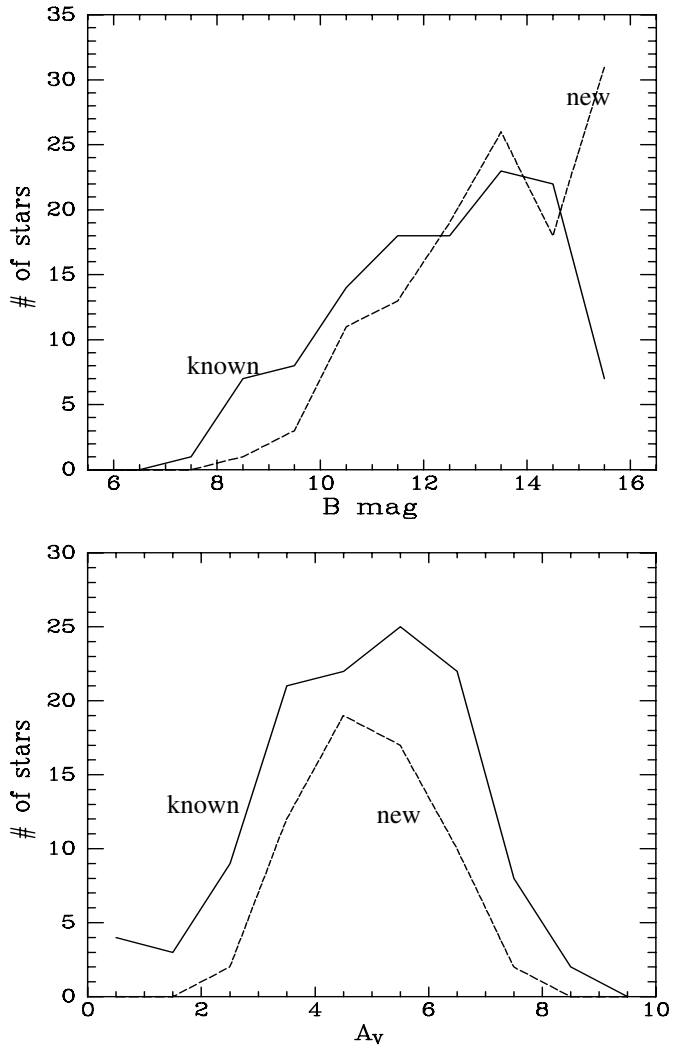

Fig. 3. *Top*: histogram of the B magnitudes of the known stars in the area selected by our criterion (solid line) and those newly found in this work (dashed line). The latter include both spectroscopically confirmed stars, and those photometrically selected but for which spectroscopy is not yet available. *Bottom*: histogram of derived extinctions toward the spectroscopically classified stars in the area, both previously known and newly identified in this work.

the spectral type versus temperature calibration is on the order of the difference between the "observational" and the "theoretical" temperature scales of Martins et al. (2005), we estimate the uncertainty in the temperature to be $\Delta \log T_{\rm eff} \simeq 0.04$ dex. We adopt 0.5 mag as the uncertainty in the dereddened V magnitude, V_0, to jointly account for the effects of possible binarity and the error introduced during the dereddening procedure by the scatter in the intrinsic color, uncertainties in the spectral classification, and possible deviations of the actual extinction law from the adopted one (e.g. Terranegra et al. 1994).

Following the derivation of $T_{\rm eff}$ and V_0 in this way, we estimated initial mass and age of each star using the evolutionary tracks of Lejeune & Schaerer (2001). The chosen set of isochrones was computed for solar metallicity, as appropriate for a nearby recently formed population, and assumed enhanced mass loss (Meynet et al. 1994), as this prescription had been shown to most closely reproduce the low luminosity of some WR stars, as well as the surface chemical composition of WC and WO stars and the ratio of the number of blue to red supergiants in the star clusters of the Magellanic Clouds. As a starting point, we adopted for all the stars a common distance modulus of $DM = 10.8$ following the extensive discussion of Hanson (2003) about the distance to Cygnus OB2, and the accurate trigonometric derivations produced by Rygl et al. (2011) for sources in the contiguous Cygnus X complex. We later discuss this assumption in the light of our results.

Initial masses and ages were assigned by measuring the distance of each star, expressed in units of the respective uncertainties in $T_{\rm eff}$ and $M_{\rm V}$ given above, to the mesh-points in the available models. The results are presented in Table 7. To estimate the accuracy of the derived initial mass and age, we computed for each star two Gaussian distributions centered at the derived $M_{\rm V}$ and $T_{\rm eff}$ values respectively, and with a variance set equal to the estimated uncertainty in those quantities. By randomly varying $M_{\rm V}$ and $T_{\rm eff}$ in consistency with the aforementioned variance, we produced best fits to the isochrones in a similar way to that outlined above. In this way, we were able to construct for each star the distributions of best-fit ages and initial masses defined by the derived $M_{\rm V}$ and $T_{\rm eff}$ and their respective uncertainties. We first removed the outliers from the distributions using a sigma-clipping (3σ) procedure, and later computed their standard deviations, which we then assumed to be the 1-σ errors in the best-fit age and initial mass. Using this procedure, we estimate the uncertainty in the best-fit age to be about 20%, while that in the best-fit initial mass is ~10% for initial masses below 30 $M_\odot$, and ~20% for higher initial masses.

5. Discussion

Figure 4 presents two views of the interstellar medium tracing the major structures in the region centered on Cygnus OB2, and covering the area where we searched for candidate O and B stars. The stars listed in Tables 1 to 4 are also superimposed. The top panel displays a map obtained with the *Midcourse Space Experiment* (MSX) satellite (Price et al. 2001) in the A (6.8–10.8 μm) band, mainly tracing thermal emission from heated dust. The bottom panel shows the view in the 21 cm radio continuum, dominated by ionized gas emission and some non-thermal sources in the region. The main structures of the interstellar medium are indicated on the images. Figure 5 shows our delimitation of the boundaries of Cygnus OB2 and OB9 and the location of all the spectroscopically classified stars. This delimitation is similar to that of Garmany & Stencel (1992) and is obviously to some extent subjective. This caveat must be kept in mind in the discussion that follows, particularly when referring to stars that are near the adopted boundaries of the associations. Stars are plotted with different symbols according to their derived ages: asterisks, four-pointed stars, and three-pointed stars indicate young (<4 Myr), intermediate (4–10 Myr), and old (>10 Myr) stars, respectively.

5.1. Cygnus OB2

The concentration of O and B stars that form the Cygnus OB2 association clearly stands out in Figs. 4 and 5. While this concentration closely matches the stellar overdensity contours derived by Knödlseder (2000) from 2MASS star counts, previously known members cluster toward higher Galactic longitudes. They define the sub-area within Cygnus OB2 that has been most studied by previous surveys (Massey & Thompson 1991) and where the very early-type, most luminous members, which led to the initial identification of Cygnus OB2 (Münch & Morgan 1953; Schulte 1956), are located together with X-ray emitting stars

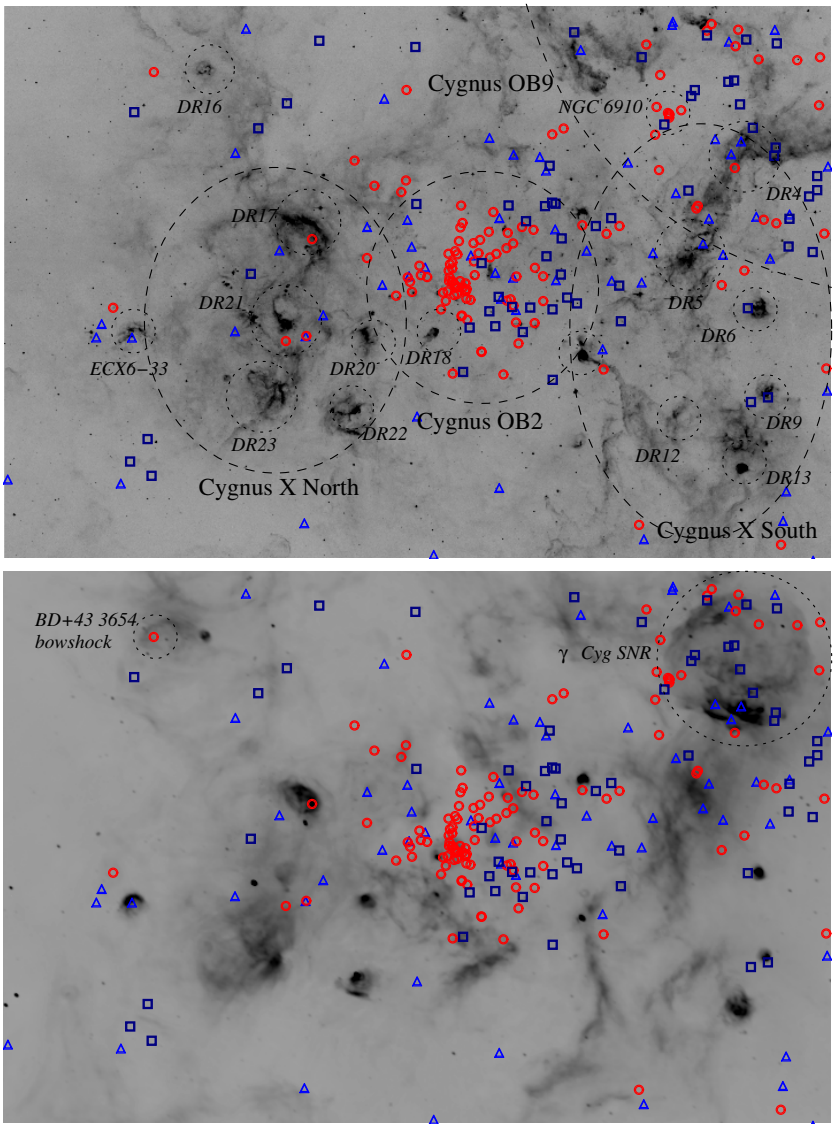

Fig. 4. Two views of the interstellar medium in the surveyed field, with the main structures in the region marked. The *top panel* presents the view in the MSX band A (6.8–10.8 μm), while the *bottom* one presents the Canadian Galactic plane survey (CGPS; Taylor et al. 2003) radio continuum emission at 21 cm. The symbols mark the stars photometrically selected in the current work after removal of those whose spectra do not confirm their O or B spectral type. Red circles are previously known O and B stars with classifications available in the literature; dark blue squares are stars newly found in the current study and spectroscopically confirmed as having O or B types; and light blue triangles are photometrically selected candidate O and B stars without available spectroscopy. The field is $6° \times 4°$, Galactic latitude increasing toward the top and Galactic longitude toward the left.

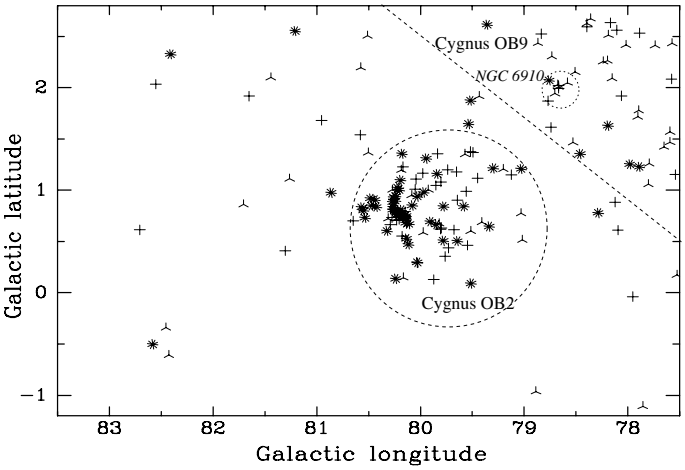

Fig. 5. Location of stars in the young (asterisks), intermediate (four-pointed stars), and old (three-pointed stars) age groups defined in the text in the surveyed area. The approximate boundaries of the associations are marked.

(Albacete Colombo et al. 2007; Wright et al. 2009). The extension of Cygnus OB2 beyond this sub-area was confirmed by the identification and classification of new early-type members by Comerón et al. (2002, 2008) and the identification of large numbers of candidate A-type stars through narrow-band imaging by Drew et al. (2008), who also noted that their distribution is offset toward lower Galactic longitudes than the main body of the association.

A comparison of the positions of stars in the $T_{\rm eff}$ vs. $M_{\rm V}$ diagram with the isochrones and evolutionary tracks used for our analysis, as shown in Fig. 6, supports the adopted distance modulus $DM = 10.8$, with only two luminosity class V stars lying slightly below the ZAMS. With very few exceptions, stars belonging to different luminosity classes are reasonably well-separated in absolute magnitude. The most discordant case appears to be J20314965+4128265, classified as O9III by Kiminki et al. (2007), although a previous classification as O9.5V by Schulte (1958) agrees more closely with its position in the $T_{\rm eff}$ vs. $M_{\rm V}$ diagram. The comparison with the isochrones indicates a considerable age spread among the members, many of which are older than 3–4 Myr. The spatial location of the stars in the different age groups shown in Fig. 5 shows that the older stars, which compose most of our sample of newly identified members, tend to be located at low Galactic longitudes. This agrees with the results of Drew et al. (2008), who assigned a representative age of 7 Myr to their sample of A-type candidate members

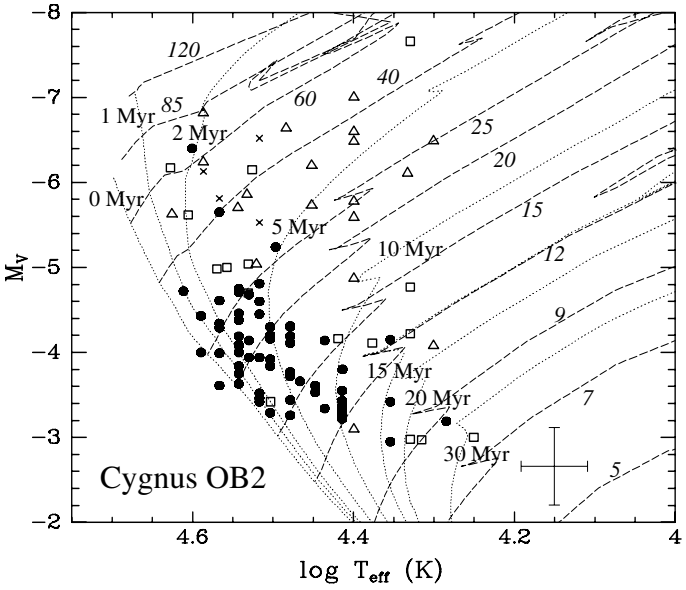

Fig. 6. Temperature-absolute magnitude diagram of stars in Cygnus OB2 selected by our criteria, assuming for the absolute magnitude a distance modulus $DM = 10.8$. Isochrones (dotted lines) and evolutionary tracks of stars of various masses (dashed lines) from Lejeune & Schaerer (2001) are plotted. Filled circles are stars of luminosities IV and V, open squares are giant stars of luminosity classes II and III, and open triangles and stars of luminosity class I. Typical uncertainties in both absolute magnitude and temperature as described in the text are represented in the lower right.

of the association using the same distance modulus that we adopt here. It is also consistent with Hanson (2003) who showed that the evolved early B-type stars in the sample of Comerón et al. (2002) tend to be displaced from region preferentially occupied by the early O stars.

Several attempts have been made to derive the initial mass function of Cygnus OB2, assisted by the abundance of very high-mass stars that comprehensively cover its uppermost end. For a power-law mass function of the form $\mathrm{d}\xi(M) = M^{-\Gamma}\,\mathrm{d}\log M$, where $\mathrm{d}\xi(M)$ is the number of stars of mass M per logarithmic mass interval, Massey & Thompson (1991) found $\Gamma = -1.0 \pm 0.1$, which was corrected to $\Gamma = -0.9 \pm 0.2$ in the re-analysis of the data by Massey et al. (1995). The region considered is the one containing the highest concentration of stars, which, as we have seen, is also the youngest one, thus less biased by evolutionary effects. A steeper slope of the mass function over a wide range of masses, $\Gamma = -1.09 \pm 0.13$, was found by Wright et al. (2010) from their sample of X-ray emitting stars. Similarly, Knödlseder et al. (2002) derived $\Gamma = -1.1 \pm 0.3$ based on a rather heterogeneous compilation of data, again based on the youngest parts of the association. Using a different approach based on 2MASS star counts and infrared colors, Knödlseder (2000) derive $\Gamma = -1.6 \pm 0.1$ assuming main sequence absolute magnitudes for O and B stars. Since the latter study also includes the older stars of the association, it is quite possible that the steeper slope with respect to the other works cited above is due to the disappearance of the most massive members that initially populated Cygnus OB2.

Trying to derive the initial mass function at the high-mass end over the whole Cygnus OB2 association from our sample is fraught with uncertainties despite our homogeneous member candidate selection criteria. Besides the significant uncertainties in the model fits possibly caused by binarity, rotation, angle of view, and the models themselves, stellar evolution has progressively depopulated the upper main sequence in the older parts of the association. Infrared surveys have revealed early-type members of Cygnus OB2 obscured by extinctions of up to a few tens of magnitudes in the visible (Comerón et al. 2002), implying that much of its stellar content remains undetected when selection criteria involving visible bands are involved. This in turn implies that there is a bias when magnitude-limited samples are considered, as the brighter stars remain detectable at higher extinction, and thus over larger volumes. When age-limited samples are considered, the slow evolution of the least massive stars on or near the main sequence makes their assignment to the different age groups difficult. Finally, both assigned masses and ages depend significantly on the precise distance adopted for the association.

In view of these difficulties, we attempted to produce a rough estimate of the initial mass function slope by using an extinction-limited sample defined by stars with $A_V < 6$, initial masses in the range $43\ M_\odot > M > 17\ M_\odot$, and age <4 Myr. The lower mass limit corresponds to the onset of incompleteness of the sample for extinctions within the range defined above, and the upper mass limit by the evolution of the most massive stars beyond the temperature range within which our color-based selection criteria can select them. The adopted limits in extinction and age thus represent a compromise, yielding a sample of 20 stars over a relatively wide mass range. Extending the mass range would require restricting the sample to younger ages in order to avoid evolutionary effects, whereas allowing for larger extinctions would require the use of a higher value of the low-mass cutoff to avoid sample incompleteness. We then divided the selected mass range into two bins, a "higher mass" bin with $N_{\rm high}$ stars having $M_i > 25\ M_\odot$ and a "lower mass" one with $N_{\rm low}$ stars, and estimated Γ from

$$\frac{N_{\rm high}}{N_{\rm low}} = \frac{M_{\rm split}^{-\Gamma} - M_{\rm high}^{-\Gamma}}{M_{\rm low}^{-\Gamma} - M_{\rm split}^{-\Gamma}},$$

where $M_{\rm low}$ and $M_{\rm high}$ are respectively the low- and high-mass ends of the mass range under consideration. Taking into account the considerable uncertainties in $N_{\rm high}$ and $N_{\rm low}$ (caused by stars that lie near the boundary between both bins, as well as stars that lie near the limits of the mass and age ranges considered), we obtained $\Gamma = -2.1 \pm 1.6$. The very large uncertainty thus renders the shape of the upper end of the initial mass function in Cygnus OB2 virtually unconstrained by our results, and illustrates the difficulties encountered in trying to determine the shape of the initial mass function in an association where significant evolution has already taken place at the high-mass end, and where interstellar extinction restricts samples selected based on visible fluxes to a small fraction of the total census.

5.1.1. BD+40 4210

Among the new Cygnus OB2 candidate members located at low Galactic latitudes, BD+40 4210 is distinctive because of its brightness, which at $K_S = 4.466$ makes it one of the brightest members of the association. We derived an absolute magnitude $M_V = -7.66$ and a mass of 54 $M_\odot$ for this star. We tentatively assigned to it a B1III:e spectral type, noting that its Balmer lines are generally much shallower than those of other B1III stars, as shown in Fig. 7. Furthermore, we observed broad emission features near 5600 Å and 5800 Å, which we tentatively ascribed to OV (λ = 5592 Å) and CIV (λ = 5805 Å). These are strong features in the spectra of some Wolf-Rayet (WR) stars of

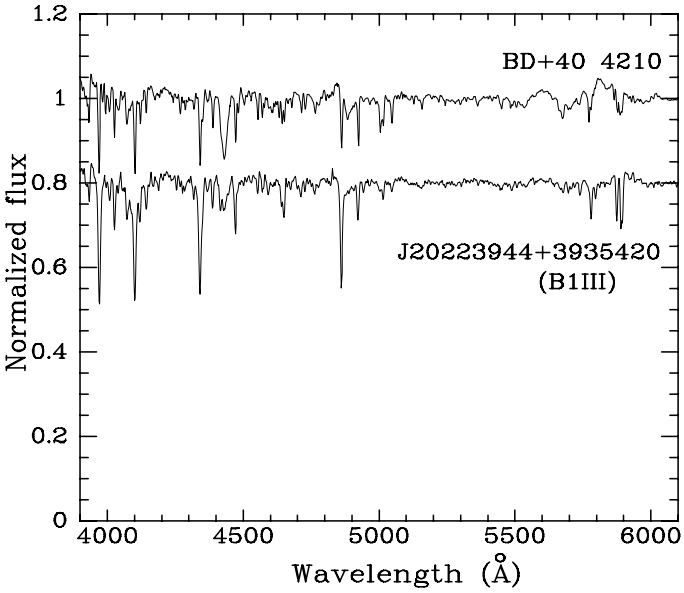

Fig. 7. Full normalized spectrum of BD+40 4210 obtained with CAFOS, showing the broad emission features near 5600 Å and 5800 Å.

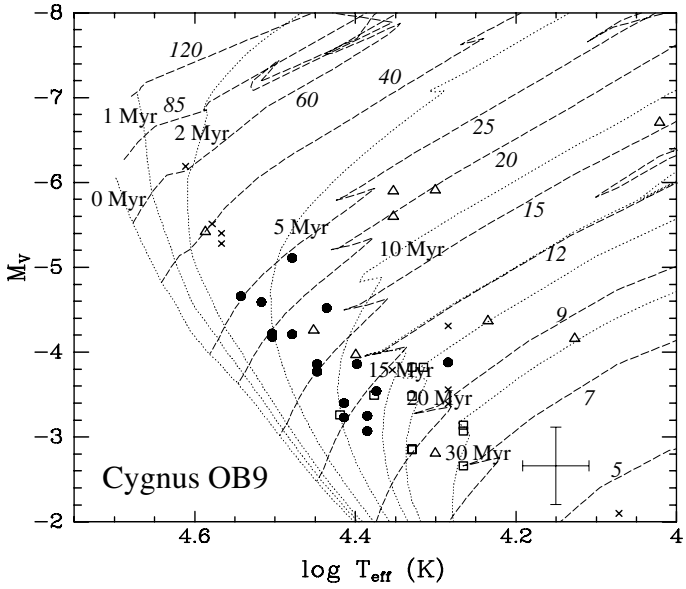

Fig. 8. Same as Fig. 6, now for the stars within the boundaries assigned to Cygnus OB9.

the WC and WO types (e.g Vreux et al. 1983; Crowther et al. 1998), although their intensity in WR stars, especially for the CIV emission, is much stronger than that observed in the spectrum of BD+40 4210. We do not observe any other obvious emission lines in the wavelength range covered by our observations, which unfortunately excludes Hα. A visible light curve of BD+40 4120 obtained over a period of 186 days at an effective wavelength close to that of the *R* band is available from the Northern Sky Variability Survey (Woźniak et al. 2004). It is characterized by an amplitude slightly below 0.1 mag and a possible period of 100 days.

The estimated temperature and luminosity of BD+40 4210 most likely place it within the S Dor instability trip and close to its high-temperature edge (Smith et al. 2004), where hot luminous blue variables (LBVs; see e.g. Humphreys & Davidson 1994; Smith et al. 2010) are located. A search for circumstellar nebulosity in archive *Spitzer* images of the region around BD+40 4210, hinting at past LBV-like eruptive episodes, yields negative results. However, it is remarkable that BD+40 4210 lies only 11′.4 (4.8 pc projected distance at 1450 pc) from the LBV candidate G79.29+0.46, which is surrounded by a ring nebula well-studied at infrared and radio wavelenghts (Wendker et al. 1991; Umana et al. 2011, and references therein). A clustering of emission-line objects was reported by Vink et al. (2008) near the same area. The central source of G79.29+0.46 with K_S = 4.33 is even brighter than BD+40 4210 and much more reddened if its near-infrared emission is entirely photospheric. It is also detected at visible wavelengths, but its classification is impossible based on the available spectroscopy (Higgs et al. 1994). The presence of two such very massive stars within a short distance, projected onto a region generally populated by post-main sequence less-massive stars, shows that star formation in this part of Cygnus OB2 has been taking place sustainedly for a long time, as discussed in Sect. 5.1.

5.2. Cygnus OB9

Cygnus OB9 spans an area of roughly 4° × 3° in Galactic longitude and latitude (Garmany & Stencel 1992). Our survey covers only the high Galactic longitude region beside Cygnus OB2. At low Galactic longitudes, Cygnus OB9 merges with Cygnus OB1, possibly forming a single vast conglomerate (Mel'nik & Efremov 1995; Schneider et al. 2007). The $T_{\rm eff}$ vs. $M_{\rm V}$ diagram of the stars in Cygnus OB9 is plotted in Fig. 8 for the same distance modulus DM = 10.8 of Cygnus OB2. This indicates that Cygnus OB9 is dominated by both intermediate – age and old stars if it is indeed located at that distance. The presence of B stars with luminosity classes I to III and the upper envelope of the distribution of luminosity class IV-V in the $T_{\rm eff}$ vs. $M_{\rm V}$ diagram presented in Fig. 8 are consistent with those estimates of the distance and the age. However, a significantly closer distance, perhaps as close as the value of 1.0 kpc (DM = 10.0) derived by Garmany & Stencel (1992) is not entirely ruled out by our results. It would imply a younger age for most of members of Cygnus OB9, and would make a physical relationship with the complex out of which Cygnus OB2 formed implausible, on the basis of the large distance between them along the line of sight. However, such a short distance would also imply that the four bona-fide supergiant members of Cygnus OB9 (the already known B0.5Ib HD 228929 and B0.5Ia HD 228882, plus the newly found B1Ia J20214410+4012529 and O5If J20223777+4140292 discussed below) are significantly less luminous than supergiants with similar spectral types in Cygnus OB2. We thus favor a common distance to both Cygnus OB2 and OB9. On the other hand, the location of the class V stars identified in Cygnus OB9 is hardly consistent with the value of DM = 11.2 derived by Delgado & Alfaro (2000) for the open cluster NGC 6910, which is normally assumed to be a member of Cygnus OB9. The discrepancy between the distance estimates to NGC 6910 and the surrounding Cygnus OB9 was already noted by Garmany & Stencel (1992), and reinforced by later studies (e.g. Kołaczkowski et al. 2004), including the results presented here. The possibility that NGC 6910 may actually be an unrelated cluster in the background of Cygnus OB9 would explain this discrepancy.

The existence of a wide range of distances among the early-type stars selected by our criteria, particularly the existence of early-type stars beyond the main body of Cygnus OB2 and possibly beyond NGC 6910, is supported by our finding of giants

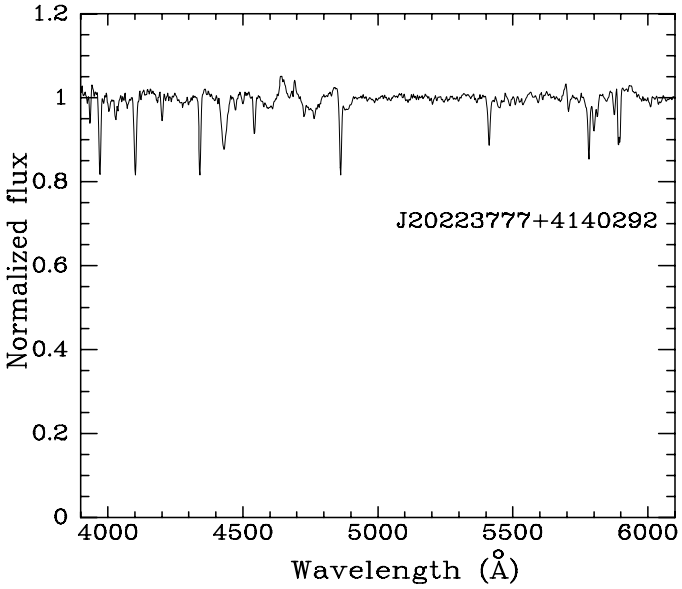

Fig. 9. Full normalized spectrum of J20223777+4140292 obtained with CAFOS, showing the emission features of NIII (4640 Å) and HeII (4686 Å).

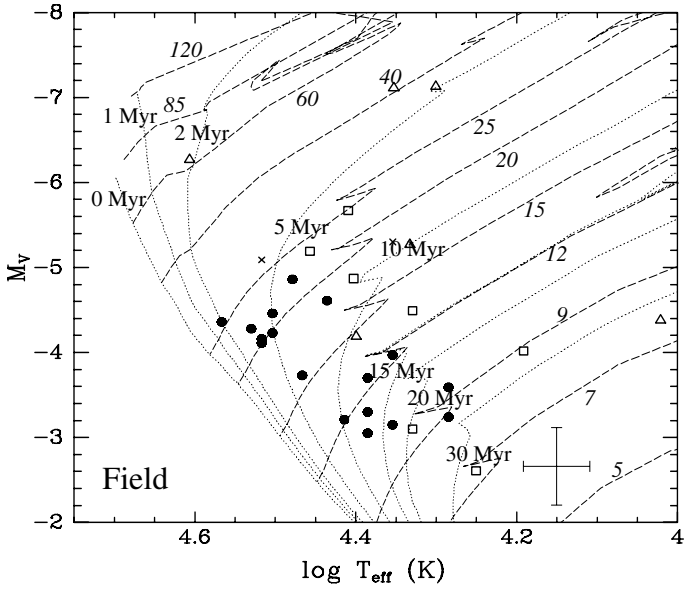

Fig. 10. Same as Fig. 6, now for the stars outside the boundaries assigned to either Cygnus OB2 or Cygnus OB9.

and supergiants with unreddened magnitudes in the same range as class V stars of similar temperature, a feature that is virtually absent from the $T_{\rm eff}$ vs. $M_{\rm V}$ diagram of Cygnus OB2. The supergiant spectral classification is doubtful for J20243872+3930301, which we tentatively classify as B0I: (owing to the noisy spectrum available), but more robust for J20215160+3959496 (B1Ib) and J20190610+4037004 (O9.7Iab). We believe that the latter two stars are likely to be in background of Cygnus OB9, and might even belong to the more distant Perseus arm. Other giants with faint derived absolute magnitudes may also be in the background.

As noted above, we find among the new members of the association a previously unnoticed O5If star, J20223777+4140292, which may be the most massive member of Cygnus OB9 at present, with an estimated initial mass of 40 $M_{\odot}$. Emission lines of NIII near 4640 Å and HeII at 4686 Å are prominent in its spectrum shown in Fig. 9. This star, together with other mid O-type stars previously known, shows that massive star formation occurred throughout the association until few million years ago.

5.3. The field population

Some of the stars previously known in the region, as well as some newly discovered ones, are found outside the boundaries assigned to either both Cygnus OB2 and OB9 or any other aggregate. The distinction between this field population and members of the associations is sometimes difficult given the lack of definite boundaries for the latter. Furthermore, at least one star in the field population, BD+43 3654, is most likely to be a runaway star recently ejected from Cygnus OB2, as shown by Comerón & Pasquali (2007), rather than a true field member. However, the number of identified stars well outside the approximate boundaries of the OB associations argues that there has been sustained massive-star formation activity in the field, and proper motions listed in the UCAC3 catalog do not provide evidence of a significant population of runaway stars.

The overall distribution of stars that we assign to the field population in the $T_{\rm eff}$ vs. $M_{\rm V}$ diagram, shown in Fig. 10, agrees with a distance modulus that is also consistent with those of the two associations. The location of the sequence defined by luminosity class V stars occupies a similar position, and stars of luminosity classes I to III appear generally above the sequence. It is thus likely that the field population is physically associated with the rest of the past and recent star forming activity in the region, as we discuss in Sect. 5.4.

Most of the field stars are B-type and belong to the intermediate and old age groups defined above, but there are also some O stars that indicate that there has been episodic massive star formation within the past 3–4 Myr. These stars bridge the gap between the older population and the current numerous star-forming regions in the Cygnus X complex, which is largely located outside the boundaries of the associations.

It is unclear whether the most luminous star in Fig. 10, the already known B0.5Iae star HD 194839, belongs to the field population, as it lies in the narrow region between Cygnus OB2 and OB9 and may also be a member of either association. Its kinematics makes it unlikely that HD 194839 is a runaway star (Tetzlaff et al. 2011), and Spitzer mid-infrared imaging of its surroundings shows no evidence of a bow shock.

5.3.1. Isolated O stars in the field

The intermediate-age and old stars in the field may be the most massive remnants of former associations or loosely bound clusters that have already dissolved, or the result of the early dynamical evolution of the existing associations. Nevertheless, the presence of a few young massive stars that are clearly independent of the known associations confirms that recent massive star formation has taken place in the field. Because of their location and youth, these stars are good test cases to investigate whether massive stars can form in isolation (Zinnecker & Yorke 2007). Some compelling cases of likely isolated formation of massive stars have been reported in the Large (Chu & Gruendl 2008) and Small Magellanic Clouds (Selier et al. 2011), and the fraction of actual isolated O stars in the Milky Way was assessed by de Wit et al. (2004, 2005) to be between 5% and 10%.

The proximity of the Cygnus region to the Sun provides some advantages over studies of more distant stars in that

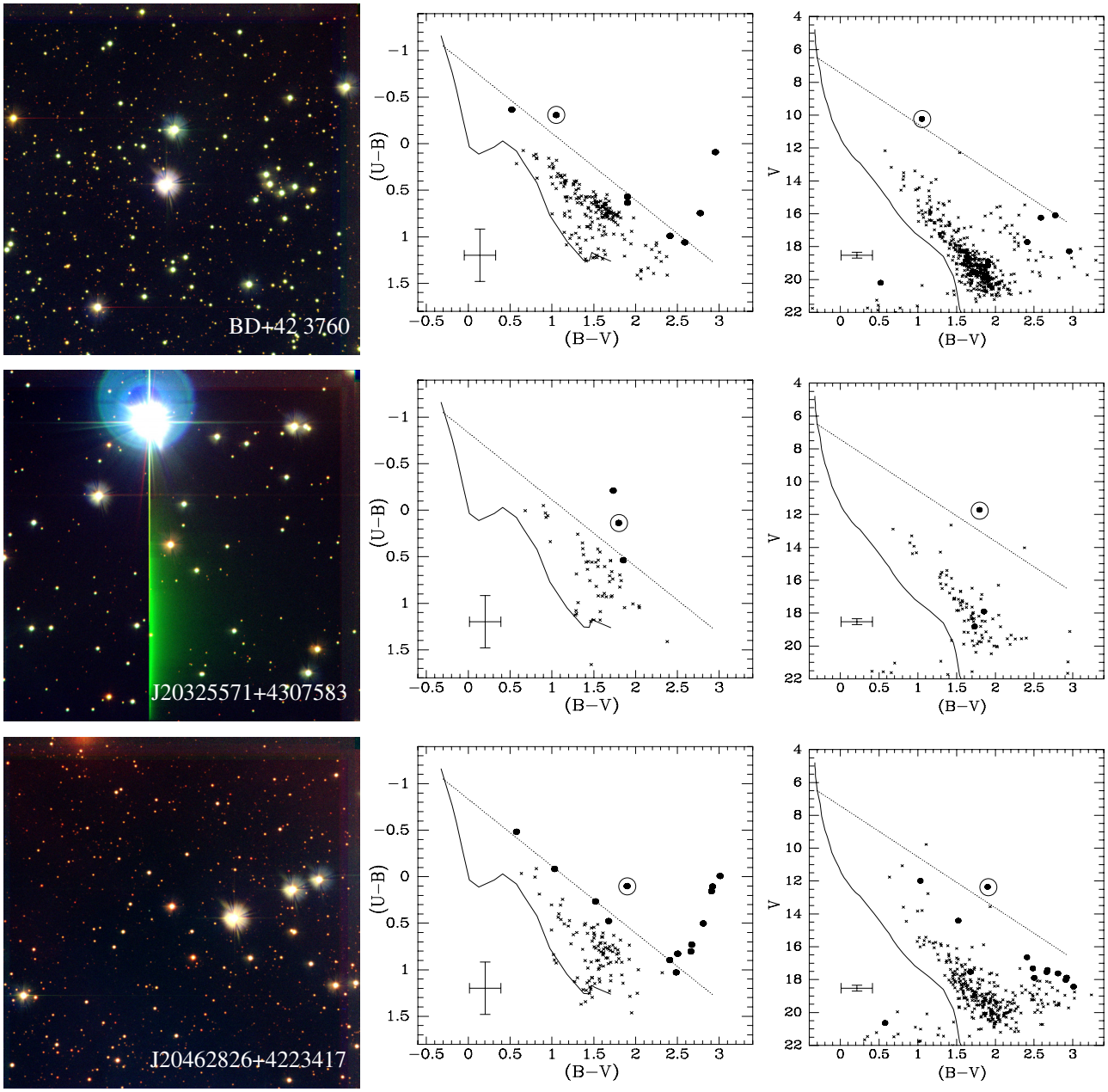

Fig. 11. Images, color–color, and color–magnitude diagrams of the fields around the late O-type stars BD+42 3760, J20325571+4307583, and J20462826+4223417. The O stars are the brightest stars slightly left of the center of the images. North is at the top and east to the left in all the images, and the field of view measures approximately 10′.1 × 10′.1. The thick dots in the color–color and color–magnitude diagrams represent intrinsically blue stars. These stars are characterized by a value of the reddening-free index $Q = (U - B) - 0.72(B - V) < -0.7$. The solid lines represent the locus of the unreddened main sequence at a distance modulus $DM = 10.8$. The dotted lines are the extinction vectors that have their origin at the position of a B0V star, with a length corresponding to an extinction $A_V = 10$ mag. The uncertainties in the photometry of the faintest stars plotted in each diagram are noted in *the lower left*.

meaningful kinematical information is available. It is also possible to check for the presence of accompanying clusters of low-mass stars that may show that the existence of the apparently isolated massive stars is actually a consequence of the random sampling of the initial mass function in the formation of relatively low-mass clusters, as proposed by Parker & Goodwin (2007).

We chose to observe the stars BD+42 3760 (O8.5V), J20325571+4307583 (O9.5V), and J20462826+4223417 (O9V), which are located more than one degree outside the adopted boundary of Cygnus OB2 (that is, more than 25 pc of projected distance). We performed *UBV* imaging of the field surrounding each of them as described in Sect. 3.2. The field of view of the instrument corresponds to a projected area of 4.2 × 4.2 pc^2 at the adopted distance of Cygnus OB2, which is adequate to cover the whole extent of a Pleiades-like cluster. *UBV* photometry provides a traditional way of identifying early-type stars through the reddening-free index $Q = (U - B) - 0.72(B - V)$, which assumes an interstellar reddening law characterized by a total-to-selective extinction ratio $R_V = A_V/E(B - V) = 3.1$. Using the main sequence colors from Drilling & Landolt (2000), early-type candidate stars in each field (spectral type approximately B1V and earlier) were identified as those having $Q < -0.7$.

Figure 11 shows images of each field, together with the color–color and color–magnitude diagrams. The central O star of each field is marked in both diagrams, as well as the candidate early-type stars identified by means of their Q indices. Although stars with $Q < -0.7$ are identified in all fields, none of them show evidence of a physical clustering of early-type stars around the targeted O star, as in all cases the early-type candidates are too faint to be early-type stars at the same distance. Indeed, stars with negative values above the threshold identifying early-type stars are always below the line indicating the location of B0V stars reddened by different amounts, which probably indicates that they are in the background.

An intriguing feature of the $(U-B),(B-V)$ diagrams of the stellar population around BD+42 3760 and J20462826+4223417 shown in Fig. 11 is the appearance in both cases of a group of stars with very red $(B-V)$ colors and unusually negative Q indices, even larger in absolute value than expected if they were very early-type, highly reddened stars. Despite the photometric uncertainties, their unusual brightness in the U band compared to their $(B-V)$ color is well-established by their very detection in U. Their faintness combined with their very red $(B-V)$ colors would place them below the U-band detection limits if they had normal photospheric colors, and that they are detected in U despite their faint and very red B, V magnitudes indicates that they have unusually high ultraviolet fluxes. The Q indices continue to be exceptionally negative even if the coefficient multiplying the $(B-V)$ term in the expression giving Q above is changed to any other reasonable value.

Rather than being background early-type candidates, the combination of red $(B-V)$ and blue $(U-B)$ colors of these stars with highly negative Q indices leads us to propose that these may be instead intermediate- or low-mass stars undergoing the intense accretion that can cause strong ultraviolet excess. If this interpretation were correct, then the color–color and color–magnitude diagrams may imply that there is a population of lower-mass stars in the fields of BD+42 3760 and J20462826+4223417. This might lend support to the hypothesis of Parker & Goodwin (2007) that apparently isolated O stars are actually the most massive members of clusters containing a normal population of lower-mass stars, in which the presence of the very massive star and the apparent absence of other O and B stars is due to the random sampling of the initial mass function. Unfortunately, a lack of spectroscopic data does not allow us to confirm the nature of these objects for the time being. Furthermore, their spatial distribution shows no obvious concentration toward the O stars, thus casting doubts on the possible physical association with them.

5.4. An overall picture of star formation history in the region

The distributions of stellar ages in the areas of Cygnus OB2, OB9, and the field are shown in Fig. 12. Reconstructing the star formation rate from those distributions would require corrections for stellar evolution and the variation in the depths reached in the different regions owing to the varying amount of extinction. Nevertheless, some general features can be appreciated from the figure. Some degree of massive-star formation has been maintained in the whole region for at least the past few tens of Myr. The star formation activity in Cygnus OB2 started to increase dramatically around 10 Myr ago, peaking at about 3 Myr ago with the formation of the dense aggregate of very hot and luminous stars that nowadays dominates the northern part of the association.

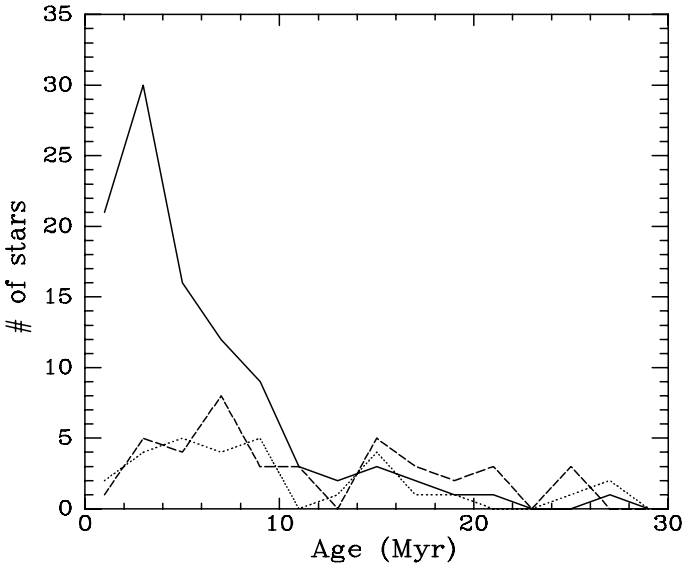

Fig. 12. Histogram of derived ages of stars within the boundaries of Cygnus OB2 (solid line), Cygnus OB9 (dashed line), and in the field (dotted line). The histograms include all the O and B stars selected by our photometric criteria for which a spectroscopic classification is available, either from the literature or the present work.

The use of the B magnitude in our criteria to select O and B stars introduces a bias in our sample against the youngest members of the region, which may be expected to be located in areas where large amounts of embedded molecular gas and dust are still present. The reality of this bias is confirmed by a comparison of our results with those of Comerón et al. (2008), where the selection of stars is based on near-infrared colors alone. The results presented in that work show a noticeable abundance of highly obscured early-type stars to the north of Cygnus OB2 (higher Galactic longitudes), coincident with the densest concentrations of molecular gas of Cygnus X North (Schneider et al. 2006), where massive-star forming regions such as DR17, DR21, DR23, and W75N are located. Almost no stars with low or moderate levels of extinction are detected in the present work in that area.

The distribution of ages within and among massive-star forming sites suggest an overall, grand-scale picture in which massive-star forming activity has been widespread in the region for tens of Myr. In the past (>10 Myr ago), most of the massive-star formation took place in the south (lower Galactic longitudes), producing the Cygnus OB9 association. Some 10 Myr ago, the main episode of star formation activity started moving north, to the southern part of Cygnus OB2, and progressed northward until its culmination about 3 Myr ago with the formation of the major concentration of massive stars in the north of Cygnus OB2. The location of embedded massive stars outside the boundaries of Cygnus OB2 reported by Comerón et al. (2008) shows that star formation continues to proceed northward at the present time in Cygnus X north, which will perhaps lead to the emergence of a new association in a few Myr from now on, as also suggested in that work. This general picture shows more complexity on smaller scales, with the existence of stars within the boundaries of Cygnus OB9 that are younger than the bulk of the stars in the southern part of Cygnus OB2, and the existence of very massive young stars such as BD+40 4210 in that same area of Cygnus OB2, or the coexistence of young O-type stars with evolved B stars in the field.

6. Conclusions

We have presented an improved census of moderately obscured O and early B stars in the wide area surrounding Cygnus OB2 that substantially increases the number of known OB stars in this region. Our selection criteria, based on the $BJHK$ magnitudes published in the USNO-B and 2MASS all-sky catalogs, produce a homogeneous sample limited by design to $B < 16$ and $K < 9$. Based on the confirmation rate that we obtain from the spectral classification of 117 stars, we estimate that approximately 80% of the objects selected as early-type candidates are indeed O or early B stars. Similarly, by comparing with samples obtained by Massey & Thompson (1991) using UBV colors, we estimate that our selection criteria recover approximately 80% of the stars in the O-B2 spectral range within the magnitude limits quoted above. This is still far from providing a complete catalog of the massive stellar content of the region, as much of it remains inaccessible to visible wavelengths owing to heavy obscuration. However, it enables studies of the large-scale star formation trends over the region and the discovery of new objects of particular interest.

Our main findings can be summarized as follows:

- A distance modulus of $DM = 10.8$ (Hanson 2003), inferred from recent trigonometric distance determinations to sources in the region (Rygl et al. 2011), is in good agreement with the position in the temperature-absolute magnitude diagram of the spectroscopically classified stars in the region. No obvious differences in distance appear between O and B stars in Cygnus OB2, Cygnus OB9, and the field. At a given temperature, main sequence, giants, and supergiants tend to appear clearly separated in the temperature-absolute magnitude diagram built by assuming a common distance modulus.
- Using individual stellar ages derived from the comparison with theoretical evolutionary tracks, the entire region is found to display a mixture of ages ranging from less than 3 Myr to over 10 Myr, thus indicating a long sustained rate of star formation.
- The presence of evolved stars in Cygnus OB2 is used to infer that a vigorous massive-star formation activity started about 10 Myr ago and culminated 3 Myr ago. The association extends beyond the area occupied by the youngest and hottest members of Cygnus OB2 where most studies have been thus far concentrated. The southern part (lower Galactic longitude) of the association is clearly older, although it does contain some very massive objects formed in the past few millions of years. The extension of the association and the older age of the southern part confirms previous findings (e.g. Drew et al. 2008; Wright et al. 2010), mostly based on less massive stellar members of the association.
- BD+40 4210, a new member of Cygnus OB2 that we have classified as B1III:e, is a remarkable member of this association. It has an estimated mass of 54 $M_\odot$ and is one of the most luminous members of the association. Its location in the temperature-luminosity diagram places it in the S Dor instability strip occupied by luminous blue variable (LBV) candidates (Smith et al. 2004). Apart from moderately intense, broad emission features near 5600 Å and 5800 Å and some likely variability at the 0.1 mag level, there is no evidence of past outbursts that would qualify BD+40 4210 as a LBV candidate. Most remarkably, BD+40 4210 is only 11′ away from G79.29+0.46, a bona-fide LBV candidate at the center of a compact ring nebula.
- If it lies at the same distance as Cygnus OB2, Cygnus OB9 is clearly older, although it does contain some members younger than 4 Myr, particularly the O5If star J20223777+4140292, which, with an estimated mass of 40 $M_\odot$ may be the most massive member of the association at present. A distance modulus of $DM = 11.2$, similar to that found by Delgado & Alfaro (2000) for the cluster NGC 6910, is inconsistent with our results, thus casting doubts on the actual membership of NGC 6910 in Cygnus OB9.
- We have discovered many new O and B stars in the field, which are not obviously related to larger structures. The position of most of these stars in the temperature-magnitude diagram is consistent with a common distance to both Cygnus OB2 and OB9. A variety of ages is found among these stars, which include some unevolved late O-type stars.
- The UBV imaging of the fields around three apparently isolated O stars does not show any evidence of clustering around them. However, the fields around two of these stars seem to contain objects with strong ultraviolet excesses, which perhaps indicates that there has been intense accretion onto young intermediate- or low-mass stars. The nature of these objects and their possible relationship with the O stars remain unclear at present.
- An overall pattern of star formation propagation is suggested by the distribution of ages in the region under study. According to this picture, massive-star formation over the past 10–20 Myr has proceeded from lower to higher Galactic longitudes, starting from Cygnus OB9, continuing in the southern part of Cygnus OB2, and increasing in its northern part about 3 Myr ago, when the compact aggregate of hot, luminous stars that dominate the current appearance of Cygnus OB2 in the visible was formed. Intense massive-star formation activity is observed to be taking place at present in the Cygnus X north complex, located further north from Cygnus OB2, suggesting that the northward propagation of star formation in the region continues. However, the more detailed view of the star formation history made possible by the availability of individual age determinations appears to follow a more intricate scenario, in which recent star formation has also taken place in the areas dominated by an older component.

Acknowledgements. We are pleased to thank the staff at the Centro Astronómico Hispano-Alemán on Calar Alto for the execution of part of the observations presented here in service mode, and for their support during our visitor observing run. We also acknowledge the excellent support provided by the staff at the Observatorio del Teide during our observing run at the IAC80 telescope. We also thank Dr. Nicola Schneider for her useful remarks on an earlier version of the manuscript, and the anonymous referee for constructive comments that helped improve the paper. This research has made use of the SIMBAD database, operated at CDS, Strasbourg, France. It also has made use of data products from the Two Micron All Sky Survey, which is a joint project of the University of Massachusetts and the Infrared Processing and Analysis Center/California Institute of Technology, funded by the National Aeronautics and Space Administration and the National Science Foundation; and of the NOMAD Catalogue produced by the United States Naval Observatory.

References

Albacete Colombo, J. F., Flaccomio, E., Micela, G., et al. 2007, A&A, 464, 211
Bochkarev, N. G., & Sitnik, T. G. 1985, Ap&SS, 108, 237
Cardelli, J. A., Clayton, G. C., & Mathis, J. S. 1989, ApJ, 345, 245
Cash, W., Charles, P., Bowyer, S., et al. 1980, ApJ, 238, L71
Cameron, D., & Nassau, J. J. 1956, ApJ, 124, 346
Chu, Y.-H., & Gruendl, R. 2008, ASP Conf. Ser., 387, 415
Comerón, F., & Pasquali, A. 2005, A&A, 430, 541
Comerón, F., & Pasquali, A. 2007, A&A, 467, L23
Comerón, F., & Torra, J. 2001, A&A, 375, 539
Comerón, F., Torra, J., & Gómez, A. E. 1998, A&A, 330, 975
Comerón, F., Pasquali, A., Rodighiero, G., et al. 2002, A&A, 389, 874
Comerón, F., Pasquali, A., Figueras, F., & Torra, J. 2008, A&A, 486, 453
Crowther, P. A., De Marco, O., & Barlow, M. J. 1998, MNRAS, 296, 367

Delgado, A. J., & Alfaro, E. J. 2000, AJ, 119, 1848
de Wit, W. J., Testi, L., Palla, F., Vanzi, L., & Zinnecker, H. 2004, A&A, 425, 937
de Wit, W. J., Testi, L., Palla, F., & Zinnecker, H. 2005, A&A, 437, 247
Douglass, G. C., Mason, B. D., Rafferty, T. J., Holdenried, R. E., & Germain, M. E. 2000, AJ, 119, 3071
Drew, J. E., Greimel, R., Irwin, M. J., & Sale, S. E. 2008, MNRAS, 387, 08
Drilling, J. S., & Landolt, A. U. 2000, in Allen's Astrophysical Quantities, ed. A. N.Cox (New York: AIP Press)
Elmegreen, B. G. 2004, in The many scales in the Universe – JENAM 2004 Astrophysics Reviews, ed. J. C. del Toro Iniesta, et al. (Dordrecht: Kluwer Acad. Publ.)
Garmany, C. D., & Stencel, R. E. 1992, A&AS, 94, 211
Guetter, H. H. 1968, PASP, 80, 197
Hanson, M. M. 2003, ApJ, 597, 957
Higgs, L. A., Wendker, H. J., & Landecker, T. L. 1994, A&A, 291, 295
Hiltner, W. A. 1956, ApJS, 2, 389
Hoag, A. A., & Applequist, N. L. 1965, ApJS, 12, 215
Humphreys, R. M. 1978, ApJS, 38, 309
Humphreys, R. M., & Davidson, K. 1994, PASP, 106, 1025
Kastner, J. H., Buchanan, C., Sahai, R., Forrest, W. J., & Sargent, B. A. 2010, AJ, 139, 1993
Kenyon, S. J., & Hartmann, L. 1995, ApJS, 101, 117
Kiminki, D. C., Kobulnicky, H. A., Kinemuchi, K., et al. 2007, ApJ, 664, 1102
Kiminki, D. C., Kobulnicky, H. A., Gilbert, I., Bird, S., & Chunev, G. 2009, AJ, 137, 4608
Klagyivik, P., & Szabados, L. 2009, A&A, 504, 959
Knödlseder, J. 2000, A&A, 360, 539
Knödlseder, J. 2003, in A Massive Star Odyssey: From Main Sequence to Supernova, ed. K. van der Hucht, A. Herrero, & C. Esteban (San Francisco: ASP), IAU Symp., 212
Knödlseder, J., Cerviño, M., Le Duigou, J.-M., et al. 2002, A&A, 390, 945
Kobulnicki, H. A., Gilbert, I. J., & Kiminki, D. C. 2010, ApJ, 710, 549
Kołaczkowski, Z., Pigulski, A., Kopacki, G., & Michalska, G. 2004, Acta Astron., 54, 33
Kraemer, K. E., Hora, J. L., Egan, M. P., et al. 2010, AJ, 139, 2319
Laugalys, V., & Strayzis, V. 2002, Baltic Astron., 11, 205
Lejeune, T., & Schaerer, D. 2001, A&A, 366, 53
Martin, P., Knödlseder, J., Meynet, G., & Diehl, R. 2010, A&A, 511, A86
Martins, F., & Plez, B. 2006, A&A, 457, 637
Martins, F., Schaerer, D., & Hillier, D. J. 2005, A&A, 436, 1049
Massey, P., & Thompson, A. B. 1991, AJ, 101, 1408
Massey, P., Johnson, K. E., & Degioia-Eastwood, K. 1995, ApJ, 454, 151
Mel'nik, A. M., & Efremov, Y. N. 1995, Astron. Lett., 21, 10
Meynet, G., Maeder, A., Schaller, G., Schaerer, D., & Charbonnel, C. 1994, A&AS, 103, 97
Morgan, W. W., Code, A. D., & Whitford, A. E. 1955, ApJS, 2, 41
Morris, P. W., Eenens, P. R. J., Hanson, M. M., Conti, P. S., & Blum, R. D. 1996, ApJ, 470, 597
Münch, L., & Morgan, W. W. 1953, ApJ, 118, 161
Negueruela, I., Marco, A., Herrero, A., & Clark, J. S. 2008, A&A, 487, 575
Odenwald, S. F., & Schwartz, P. R. 1993, ApJ, 405, 706
Parker, R. J., & Goodwin, S. P. 2007, MNRAS, 380, 1271
Petrie, R. M., Crampton, D., Leir, A., & Jounger, S. 1973, Publ. Dominion Astroph. Obs., 14, 151
Pettersen, B. R., Tsvetkov, M. K., Hawley, S. L., Coleman, L. A., & Amirkhanian, A. S. 1988, Astrofizika, 29, 67
Price, S. D., Egan, M. P., Carey, S. J., Mizuno, D. R., & Kuchar, T. A. 2001, AJ, 121, 2819
Reipurth, B., & Schneider, N. 2008, in Handbook of Star Formation Regions, ed. B. Reipurth, ASP Monograph (San Francisco: ASP)
Rygl, K. L. J., Brunthaler, A., Sanna, A., et al. 2012, A&A, 539, A79
Rieke, G. H., & Lebofsky, M. J. 1985, ApJ, 288, 618
Sato, K., & Kuji, S. 1990, A&AS, 85, 1069
Schneider, N., Bontemps, S., Simon, R., et al. 2006, A&A, 458, 855
Schneider, N., Simon, R., Bontemps, S., Comerón, F., & Motte, F. 2007, A&A, 474, 873
Schulte, D. H. 1956, ApJ, 124, 530
Schulte, D. H. 1958, ApJ, 128, 41
Selier, R., Heydari-Malayeri, M., & Gouliermis, D. A. 2011, A&A, 529, A40
Skrutskie, M. F., Cutri, R., Stiening, R., et al. 2006, AJ, 131, 1163
Smith, N., Vink, J. S., & de Koter, A. 2004, ApJ, 615, 475
Smith, N., Povich, M. S., Whitney, B. A., et al. 2010, MNRAS, 406, 952
Stankov, A., & Handler, G. 2005, ApJS, 158, 193
Stetson, P. B. 1987, PASP, 99, 191
Taylor, A. R., Gibson, S. J., Peracaula, M., et al. 2003, AJ, 125, 3145
Terranegra, L., Chavaria-K, C., Diaz, S., & González Patiño, D. 1994, A&AS, 104, 557
Tetzlaff, N., Neuhäuser, R., & Hohle, M. M. 2011, MNRAS, 410, 190
Tokunaga, A. T. 2000, in Allen's Astrophysical Quantities, ed A. N. Cox (New York: AIP Press)
Torres-Dodgen, A. V., Carroll, M., & Tapia, M. 1991, MNRAS, 249, 1
Umana, G., Buemi, C. S., Trigilio, C., et al. 2011, ApJ, 739, L11
Uyaniker, B., Fürst, E., Reich, W., Aschenbach, B., & Wielebinski, R. 2001, A&A, 371, 675
Vijapurkar, J., & Drilling, J. S. 1993, ApJS, 89, 293
Vink, J. S., Drew, J. E., Steeghs, D., et al. 2008, MNRAS, 387, 308
Vogt, S. S. 1973, AJ, 78, 389
Vreux, J. M., Dennefeld, M., & Andrillat, Y. 1983, A&AS, 54, 437
Walborn, N. R., & Fitzpatrick, E. L. 1990, PASP, 102, 1094
Walker, G. A. H., & Hodge, S. M. 1968, PASP, 80, 290
Wendker, H. J., Higgs, L. A., & Landecker, T. L. 1991, A&A, 241, 551
Woźniak, P. R., Vestrand, W. T., Akerlof, C. W., et al. 2004, AJ, 127, 2436
Wright, N. J., & Drake, J. J. 2009, ApJS, 184, 84
Wright, N. J., Drake, J. J., Drew, J. E., & Vink, J. S. 2010, ApJ, 713, 871
Zacharias, N., Monet, D. G., Levine, S. E., et al. 2004, A&AS, 205, 4815
Zacharias, N., Finch, C., Girard, T., et al. 2010, AJ, 139, 2184
Zinnecker, H., & Yorke, H. W. 2007, ARA&A, 45, 481

Pages 15 to 23 are available in the electronic edition of the journal at http://www.aanda.org

Table 1. Known, spectroscopically classified O and B stars in the region.

Object	α (2000)	δ	B (USNO B)	J	H (2MASS)	K_S	Sp. type	Source	Notes
HD 228821	20 18 04.930	+40 06 06.80	9.254	8.874	8.951	8.928	B8	1	(a)
HD 193426	20 18 39.749	+40 13 36.89	8.809	5.014	4.650	4.357	B9Ia	2	
HD 228882	20 18 57.784	+40 42 18.52	10.202	6.522	6.181	5.966	B05Ia	2	
HD 228911	20 19 21.712	+40 53 16.46	8.726	7.801	7.773	7.771	B2	1	(b)
HD 228919	20 19 27.908	+40 27 42.09	10.174	8.339	8.216	8.143	B1IV	2	
HD 228928	20 19 32.709	+40 39 13.75	10.406	7.596	7.295	7.148	B2Ib:nn	2	
HD 228929	20 19 36.542	+39 54 41.80	10.689	6.866	6.494	6.284	B0.5Ib	2	
HD 228941	20 19 40.169	+40 53 19.19	9.182	8.146	8.084	8.082	B3	1	
HD 193945	20 21 25.823	+41 11 39.56	9.053	6.995	6.856	6.773	B0Vnn	2	
HD 194092	20 22 05.443	+40 59 08.17	8.354	7.972	8.013	8.022	B0.5III	2	
HD 194194	20 22 44.760	+40 42 52.63	8.160	8.081	8.128	8.169	B2III	2	
NGC 6910 #16	20 23 07.301	+40 46 55.25	11.285	8.512	8.265	8.124	B3	3	(c)
NGC 6910 #14	20 23 07.575	+40 46 08.87	10.880	8.491	8.237	8.149	B0.5V	3	(c)
BD+40 4146	20 23 10.464	+40 45 52.34	10.288	7.731	7.467	7.361	B3	6	
HD 229196	20 23 10.784	+40 52 29.85	9.260	6.353	6.079	5.917	O5	2	
BD+40 4148	20 23 14.549	+40 45 19.07	11.051	8.167	7.929	7.795	O9.5:V	4	
HD 229202	20 23 22.840	+40 09 22.53	10.309	7.604	7.429	7.312	O8V:	2	
BD+38 4058	20 23 28.531	+39 20 59.05	11.457	8.157	7.912	7.775	B0V	5	
J20240515+4046035	20 24 05.154	+40 46 03.51	12.308	8.653	8.325	8.158	B0.5V	7	
HD 229250	20 24 11.733	+39 40 41.54	10.887	7.267	6.984	6.817	O7	5	
BD+39 4168	20 24 21.475	+39 46 03.90	10.872	7.343	6.963	6.771	O7	5	
BD+40 4159	20 25 06.521	+40 35 49.78	11.343	7.941	7.645	7.490	O9V	7	
BD+39 4177	20 25 22.122	+40 13 01.09	9.890	6.857	6.633	6.512	O6.5	5	
BD+39 4179	20 25 28.893	+40 12 54.13	12.202	9.074	8.752	8.642	B0III	7	
HD 194779	20 25 55.077	+41 20 11.73	7.974	7.182	7.155	7.128	B3II	2	
BD+39 4189	20 26 20.922	+39 40 10.06	10.360	7.115	6.803	6.584	B2p?e?	5	
HD 194839	20 26 21.545	+41 22 45.65	8.342	5.240	4.961	4.724	B0.5Iae	2	
LSII+39 53	20 27 17.572	+39 44 32.60	10.822	8.096	7.833	7.702	O7V:	8	
BD+38 4098	20 27 33.010	+38 46 19.62	9.681	6.875	6.663	6.500	B9Ib	2	
BD+40 4179	20 27 43.616	+40 35 43.51	10.115	8.419	8.327	8.256	O8V:	2	
BD+41 3762	20 28 15.212	+42 25 39.14	11.123	8.288	8.002	7.852	B2V	2	
BD+40 4185	20 28 15.471	+40 38 19.81	10.474	8.026	7.859	7.786	B0V:	2	
HD 195213	20 28 32.027	+40 49 02.88	9.504	6.668	6.440	6.258	O7	2	
J20294666+4105083	20 29 46.672	+41 05 08.32	12.870	9.033	8.636	8.457	B0.5V(n) sb2?	9	
J20295701+4109538	20 29 57.010	+41 09 53.84	13.013	9.119	8.702	8.452	B0V	9	
J20300788+4123504	20 30 07.877	+41 23 50.44	15.640	9.397	8.739	8.365	O8V	10	
V1827 Cyg	20 30 27.300	+41 13 25.13	14.740	7.630	6.850	6.445	Ofpe	10	
J20303970+4108489	20 30 39.701	+41 08 48.80	12.429	6.928	6.328	5.980	B0.7Ib	9	
J20303980+4136506	20 30 39.805	+41 36 50.63	14.100	9.098	8.574	8.313	O6V	11	
J20305111+4120218	20 30 51.115	+41 20 21.78	15.290	9.794	9.193	8.889	B0V	11	
J20305552+4109575	20 30 55.516	+40 54 54.03	14.060	9.247	8.759	8.474	B0V	10	
J20305772+4109575	20 30 57.727	+41 09 57.51	14.610	9.093	8.514	8.198	O9.5V	10	
J20310019+4049497	20 31 00.204	+40 49 49.70	12.077	8.378	8.016	7.826	O7V((f))	9	
J20310838+4202422	20 31 08.376	+42 02 42.25	13.102	7.828	7.292	7.023	O9.7II	9	
VI Cyg 1	20 31 10.543	+41 31 53.53	12.486	7.968	7.556	7.365	O9V	2	
J20311833+4121216	20 31 18.329	+41 21 21.65	14.130	8.607	8.046	7.746	O9V	11	
VI Cyg 2	20 31 22.026	+41 31 28.40	11.711	8.075	7.750	7.628	B1Ib:	2	
J20312210+4112029	20 31 22.101	+41 12 02.87	14.420	9.397	8.928	8.629	B2V	10	
J20313338+4122490	20 31 33.378	+41 22 49.02	14.970	9.744	9.222	8.939	B1V	11	
J20313690+4059092	20 31 36.911	+40 59 09.06	15.380	7.913	7.208	6.811	O7Ib(f)	10	
J20313693+4201218	20 31 36.921	+42 01 21.79	12.118	7.355	6.956	6.657	B0.7Ib	9	
VI Cyg 3	20 31 37.506	+41 13 20.99	11.633	6.498	6.001	5.748	O9:	2	
J20314215+4225532	20 31 42.151	+42 25 53.26	13.575	6.245	5.476	5.057	B1Ib	7	
J20314540+4118267	20 31 45.403	+41 18 26.73	13.620	8.065	7.552	7.259	O8I	11	
J20314605+4043246	20 31 46.053	+40 43 24.61	13.840	8.910	8.484	8.257	B0.5IV	9	
J20314965+4128265	20 31 49.658	+41 28 26.50	12.567	9.074	8.768	8.634	O9III	11	
BD+41 3794	20 32 02.204	+42 12 26.15	11.399	7.544	7.251	7.040	B0.2III	7	
J20320689+4117570	20 32 06.877	+41 17 56.97	15.130	9.624	9.070	8.786	B3V	11	
VI Cyg 4	20 32 13.822	+41 27 12.01	11.231	7.582	7.248	7.105	O7IIIf	11	
LS III +41 30	20 32 16.563	+41 25 35.67	12.249	8.714	8.389	8.185	O9V	11	
J20322734+4055184	20 32 27.339	+40 55 18.25	13.950	8.622	8.156	7.879	B2V	9	
LS III +41 32	20 32 27.738	+41 28 52.26	11.986	9.191	8.895	8.766	B0Ib	11	
J20323033+4034332	20 32 30.310	+40 34 33.22	14.000	7.892	7.365	7.070	O9.5IV	9	
J20323154+4114082	20 32 31.531	+41 14 08.18	14.720	7.817	7.094	6.664	O7.5Ib-II(f)	10	
J20323498+4052390	20 32 34.848	+40 52 39.46	14.980	9.435	8.894	8.605	B0.2V	10	

Table 1. continued.

Object	α (2000)	δ	B (USNO B)	J	H (2MASS)	K_S	Sp. type	Source	Notes
J20323486+4056174	20 32 34.865	+40 56 17.35	14.930	9.382	8.858	8.564	O8V	10	
J20323843+4040445	20 32 38.441	+40 40 44.48	15.330	8.347	7.705	7.383	O8III	10	
VI Cyg 16	20 32 38.571	+41 25 13.79	11.857	8.194	7.918	7.716	O8V(n)	9	
VI Cyg 6	20 32 45.450	+41 25 37.57	11.670	7.953	7.617	7.421	O8V	11	
J20325002+4123446	20 32 50.016	+41 23 44.70	12.427	8.579	8.188	7.982	O8V	11	
J20325919+4124254	20 32 59.057	+41 24 24.79	12.820	8.885	8.523	8.314	O8V	11	
J20325964+4115146	20 32 59.633	+41 15 14.66	14.940	9.047	8.451	8.144	B0V	11	
J20330292+4117431	20 33 02.913	+41 17 43.16	14.500	8.718	8.165	7.873	O8V	11	
J20330292+4047254	20 33 02.928	+40 47 25.29	14.400	7.251	6.632	6.274	O8II((f))	9	
J20330879+41131	20 33 08.818	+41 13 17.93	13.290	7.110	6.540	6.225	O4III	11	(d)
V2186 Cyg	20 33 10.502	+41 22 22.44	13.910	9.537	9.113	8.897	B0V	11	(e)
VI Cyg 9	20 33 10.735	+41 15 08.22	12.512	6.468	5.897	5.570	O5If	11	
J20331326+4113287	20 33 13.264	+41 13 28.67	15.020	8.982	8.346	8.009	O6V	11	
J20331369+4113057	20 33 13.688	+41 13 05.77	14.060	9.034	8.559	8.280	O8V	11	
VI Cyg 7	20 33 14.110	+41 20 21.91	11.857	7.248	6.818	6.611	O3If	11	
VI Cyg 23	20 33 15.685	+41 20 18.75	12.920	9.333	8.935	8.724	O9V	11	
VI Cyg 8D	20 33 16.256	+41 19 00.16	12.580	8.842	8.423	8.239	O8.5V	11	
J20331748+4117093	20 33 17.483	+41 17 09.35	13.090	8.354	7.889	7.649	O7V	11	
VI Cyg 8C	20 33 17.982	+41 18 31.19	11.059	7.165	6.792	6.579	O5III	11	
J20331803+4121366	20 33 18.035	+41 21 36.67	12.698	8.744	8.315	8.113	O8V	11	
J20332101+4117401	20 33 21.016	+41 17 40.11	13.630	9.301	8.899	8.672	O9V	11	
J20332346+4109130	20 33 23.471	+41 09 12.90	13.500	7.025	6.380	6.050	O5.5V	11	
J20332557+4133269	20 33 25.569	+41 33 26.88	12.840	8.168	7.748	7.523	O8.5V	12	
J20332674+4110595	20 33 26.756	+41 10 59.42	14.240	8.971	8.434	8.165	O8.5V	11	
J20333030+4135578	20 33 30.316	+41 35 57.88	13.790	8.385	7.839	7.568	O8V	12	
J20333078+4115226	20 33 30.791	+41 15 22.70	12.645	6.493	5.891	5.542	B1I	11	
BD+43 3654	20 33 36.079	+43 59 07.38	11.245	6.636	6.198	5.973	O4If	13	(f)
J20333700+4116113	20 33 36.994	+41 16 11.31	13.530	8.683	8.168	7.929	B0V	11	
J20333821+4041064	20 33 38.213	+40 41 06.35	14.700	6.904	6.170	5.745	B0Ia	10	
J20333910+4119258	20 33 39.102	+41 19 25.98	12.858	7.230	6.745	6.482	B0Iab	11	(g)
J20334086+4130189	20 33 40.863	+41 30 18.95	13.680	9.263	8.866	8.614	O7V	11	
VI Cyg 10	20 33 46.112	+41 33 01.00	11.197	6.294	5.839	5.582	O9.5Ia	2	
J20334783+4120415	20 33 47.831	+41 20 41.37	13.051	7.986	7.487	7.209	B1III	11	
BD+37 3976	20 33 49.752	+38 17 00.06	10.852	8.686	8.553	8.447	B1.5Vn	2	
J20335952+4117354	20 33 59.527	+41 17 35.46	13.180	8.534	8.140	7.889	O9.5V	11	
J20340435+4108078	20 34 04.349	+41 08 07.91	14.850	9.685	9.163	8.887	B1V	11	
J20340486+4105129	20 34 04.851	+41 05 11.76	14.530	9.560	9.095	8.836	O9V	11	
J20340601+4108090	20 34 06.017	+41 08 09.13	14.840	9.047	8.494	8.154	O9.5V	11	
VI Cyg 11	20 34 08.514	+41 36 59.39	11.221	6.650	6.226	5.990	O5I	11	
J20341350+4135027	20 34 13.511	+41 35 02.86	13.562	8.550	8.148	7.921	O7V	11	
J20342193+4117016	20 34 21.934	+41 17 01.66	13.660	8.388	7.878	7.602	O8III + O8III	14	(h)
J20342894+4156171	20 34 28.941	+41 56 17.09	14.090	9.019	8.453	8.207	O9V	15	(i)
J20342959+4131455	20 34 29.599	+41 31 45.49	13.369	7.560	7.030	6.709	O7V	11	
J20344410+4051584	20 34 44.146	+40 51 58.67	14.740	8.404	7.796	7.448	O6.5III(f)	10	
J20344471+4051465	20 34 44.716	+40 51 46.73	13.815	6.683	6.062	5.731	B0Ia	10	
J20345606+4038179	20 34 56.057	+40 38 17.92	13.540	7.440	6.859	6.545	O9.7Iab	9	
J20345878+4136174	20 34 58.781	+41 36 17.35	12.865	7.193	6.655	6.356	B0 Ib(n) sb2?	9	
LS III +42 17	20 35 10.623	+42 20 22.83	11.692	7.845	7.504	7.318	B1III	7	
J20360451+4056129	20 36 04.500	+40 56 13.01	13.950	8.568	7.968	7.685	O5V((f))	9	
HD 196489	20 36 24.259	+39 11 40.70	8.614	8.164	8.176	8.179	B3V	16	
J20382040+4156563	20 38 20.413	+41 56 56.51	15.340	7.840	7.082	6.686	B0II	7	
J20385918+4202395	20 38 59.181	+42 02 39.45	13.270	8.684	8.186	7.906	B0Ib	7	
BD+42 3835	20 42 06.863	+43 11 03.72	9.975	7.294	7.049	6.928	O9p...	2	
HD 199021	20 52 53.207	+42 36 27.87	8.919	7.180	7.067	6.999	B0V	17	

Notes. (a) Variable (Petrie et al. 1973); (b) Eclipsing binary; (c) β Cep variable (Stankov & Handler 2005); (d) Binary; (e) Eclipsing binary (Kiminki et al. 2007); (f) Runaway with bow shock (Comerón & Pasquali 2007); (g) V1393 Cyg; (h) Binary (Kiminki et al. 2009); (i) Runaway with bow shock (Kobulnicki et al. 2010).

References. *Spectral type source*: 1) Petrie et al. (1973); 2) Morgan et al. (1955); 3) Stankov & Handler (2005); 4) Hoag & Applequist (1965); 5) Hiltner (1956); 6) Walker & Hodge (1968); 7) Comerón et al. (2008); 8) Vijapurkar & Drilling (1993); 9) Hanson (2003); 10) Negueruela et al. (2008); 11) Kiminki et al. (2007); 12) Massey & Thompson (1991); 13) Comerón & Pasquali (2007); 14) Kiminki et al. (2009); 15) Kobulnicki et al. (2010); 16) Sato & Kuji (1990); 17) Guetter (1968).

Table 2. Stars with previous classification reobserved by us.

Name	Published classification	Our classification
J20240515+4046035	B0.5V	B0.5V
BD+40 4159	O9V	O9III
J20303980+4136506	O6V	O6.5V
J20305552+4109575	B0V	B0Ib
J20305772+4109575	O9.5V	O9V
J20311833+4121216	O9V	O9.5V
J20312210+4112029	B2V	B0.2III
J20313338+4122490	B1V	B0.5V
J20314540+4118267	O8I	O8V
J20320689+4117570	B3V	B0:II
J20323154+4114082	O7.5Ib-II(f)	O6.5Ib(f)
J20323498+4052390	B0.2V	B0.2IV
J20333821+4041064	B0Ia	B1Ib
J20340435+4108078	B1V	B1III
J20340486+4105129	O9V	O8.5V
J20340601+4108090	O9.5V	B0V
J20342894+4156171	O9V	O9V

Table 3. New O and B stars.

Object	α (2000)	δ	B (USNO B)	J	H (2MASS)	K_S	Sp. type	Notes
J20183413+4025045	20 18 34.130	+40 25 04.47	14.880	8.172	7.747	7.541	B0.2IV	
J20190610+4037004	20 19 06.102	+40 37 00.39	13.330	8.576	8.115	7.880	O9.7Iab	
J20194916+4052090	20 19 49.156	+40 52 08.99	12.800	8.598	8.209	7.987	O9.5V	
J20203933+4031176	20 20 39.334	+40 31 17.64	13.550	9.551	9.137	8.927	B1.5V	
J20204933+4033027	20 20 49.333	+40 33 02.73	14.570	9.524	9.061	8.808	B1.5V	
J20211677+4023162	20 21 16.773	+40 23 16.19	14.080	9.404	8.902	8.654	B2III	
J20214410+4012529	20 21 44.103	+40 12 52.91	13.200	7.106	6.476	6.137	B1Ia	
J20214868+4043005	20 21 48.682	+40 43 00.45	11.694	8.873	8.629	8.484	B1V	
J20215115+3937515	20 21 51.149	+39 37 51.47	11.789	8.269	7.975	7.834	B3V	
J20215160+3959496	20 21 51.600	+39 59 49.61	12.081	9.284	9.014	8.874	B1Ib	
J20215593+4110129	20 21 55.930	+41 10 12.92	12.470	9.371	9.084	8.916	B1III	
J20220454+4042487	20 22 04.541	+40 42 48.73	11.811	8.725	8.462	8.280	B1III	
J20220879+3958161	20 22 08.793	+39 58 16.07	12.441	8.509	8.148	7.970	B1II	
J20221729+3934215	20 22 17.286	+39 34 21.50	14.700	8.419	7.750	7.421	B5Ia	
J20223777+4140292	20 22 37.766	+41 40 29.23	11.783	7.509	7.080	6.829	O5If	
J20223944+3935420	20 22 39.442	+39 35 42.02	11.719	8.329	8.047	7.914	B1III	
J20233375+4045199	20 23 33.752	+40 45 19.93	12.461	9.366	9.055	8.906	B1III	1
J20234624+3937078	20 23 46.238	+39 37 07.83	11.986	8.406	8.157	7.998	B0.7IV	
J20241767+3920326	20 24 17.666	+39 20 32.56	12.515	9.160	8.838	8.700	B1V	
J20243872+3930301	20 24 38.720	+39 30 30.10	15.910	9.213	8.559	8.247	B0I:	
J20250591+4020124	20 25 05.912	+40 20 12.44	12.516	9.265	9.018	8.885	B2III	
J20264025+4233221	20 26 40.251	+42 33 22.09	12.796	9.504	9.172	8.991	B2II	
J20272428+4115458	20 27 24.282	+41 15 45.82	12.624	9.365	9.027	8.830	O9.5V	
J20272553+3929246	20 27 25.529	+39 29 24.58	12.760	8.488	8.126	7.917	O9.5V	
J20273982+4040384	20 27 39.821	+40 40 38.35	11.970	8.963	8.691	8.578	B1V	
J20281539+4044046	20 28 15.392	+40 44 04.57	12.145	8.219	7.846	7.632	B1III	
J20282772+4104018	20 28 27.723	+41 04 01.80	14.220	9.364	8.867	8.636	B0.5V	
J20283039+4105290	20 28 30.385	+41 05 29.04	13.365	7.094	6.472	6.125	OC9.7Ia	
BD+42 3760	20 28 40.812	+43 08 58.46	10.862	8.065	7.838	7.725	O8.5V	
J20284657+4107069	20 28 46.566	+41 07 06.86	15.290	9.700	9.136	8.834	B2II	
J20292449+4052599	20 29 24.485	+40 52 59.85	13.860	8.873	8.333	8.050	B0.2IV	
J20293473+4020381	20 29 34.728	+40 20 38.09	14.020	9.324	8.835	8.570	B1V	
J20293480+4120089	20 29 34.798	+41 20 08.93	15.430	9.454	8.819	8.488	O9.5V	
J20294060+4109585	20 29 40.601	+41 09 58.54	13.540	9.406	8.991	8.776	B1[e]	
J20294195+3859342	20 29 41.952	+38 59 34.16	13.440	9.054	8.587	8.407	B0.2V	
J20301273+3904216	20 30 12.732	+39 04 21.59	14.580	9.593	9.119	8.885	B1V	
J20301839+4053466	20 30 18.391	+40 53 46.56	15.150	8.921	8.270	7.963	O9V	
J20303297+4044024	20 30 32.965	+40 44 02.41	13.190	9.190	8.808	8.634	B1V	
J20303833+4010538	20 30 38.329	+40 10 53.84	15.350	9.602	9.038	8.756	B1V	
BD+40 4210	20 31 04.659	+40 30 56.93	12.201	5.469	4.833	4.466	B1III:e	
J20310700+4035537	20 31 07.003	+40 35 53.73	14.410	9.609	9.182	8.928	B1III	
J20312725+4304227	20 31 27.253	+43 04 22.67	13.690	9.035	8.583	8.343	B1.5V	
J20313853+4152585	20 31 38.532	+41 52 58.46	14.010	9.627	9.216	8.968	B1.5V	
J20314885+4038001	20 31 48.848	+40 38 00.05	14.180	9.551	9.110	8.895	B1II	
J20315961+4114505	20 31 59.609	+41 14 50.45	14.460	9.117	8.579	8.326	O7V	
J20321568+4046170	20 32 15.679	+40 46 17.00	15.110	9.609	9.117	8.826	B0.2IV	
BD+40 4223	20 32 39.057	+41 00 07.78	12.208	6.035	5.487	5.157	B0Ia	
J20323951+4052475	20 32 39.507	+40 52 47.46	15.050	8.884	8.289	8.004	B0:V:	
J20325571+4307583	20 32 55.713	+43 07 58.26	15.130	8.348	7.938	7.722	O9.5V	
J20331130+4042337	20 33 11.300	+40 42 33.73	15.660	9.084	8.435	8.105	B0:III:	
J20331870+4059379	20 33 18.696	+40 59 37.92	15.270	9.205	8.591	8.140	B0.5IIIe	
J20333822+4053412	20 33 38.218	+40 53 41.19	13.530	8.028	7.496	7.235	B0Ib	
J20335842+4019411	20 33 58.417	+40 19 41.13	15.480	7.960	7.274	6.928	O9:	
J20341605+4102196	20 34 16.046	+41 02 19.59	15.100	9.409	8.830	8.517	O9.5V	
J20352227+4355305	20 35 22.266	+43 55 30.46	13.980	8.416	7.887	7.588	B0.2IV	
J20354703+4053012	20 35 47.026	+40 53 01.17	13.780	9.539	9.164	8.968	B2V	
J20374323+4232334	20 37 43.232	+42 32 33.40	14.620	9.703	9.173	8.896	B1III	
J20452110+4223514	20 45 21.103	+42 23 51.37	15.280	9.769	9.217	8.939	B2V	
J20462289+4212311	20 46 22.892	+42 12 31.07	13.052	8.808	8.468	8.221	B3V	
J20462826+4223417	20 46 28.255	+42 23 41.74	13.500	8.793	8.327	8.085	O9V	

Notes. 1 β Cep variable (Stankov & Handler 2005).

Table 4. Other candidate O and B stars without spectral classification.

Object	α (2000)	δ	B (USNO B)	J	H (2MASS)	K_S	Notes
J20181090+4029063	20 18 10.898	+40 29 06.29	14.940	9.343	8.709	8.399	
J20193232+4042447	20 19 32.323	+40 42 44.72	12.890	9.288	8.894	8.692	
HD 228973	20 20 07.350	+41 07 46.72	10.340	7.922	7.760	7.684	1
J20201435+4107155	20 20 14.349	+41 07 15.45	12.412	8.627	8.352	8.240	
J20211924+3936230	20 21 19.240	+39 36 22.98	12.732	8.488	8.096	7.886	
J20222481+4013426	20 22 24.814	+40 13 42.55	13.620	9.034	8.614	8.410	
J20225451+4023314	20 22 54.508	+40 23 31.39	13.107	9.175	8.771	8.601	
J20230183+4014029	20 23 01.830	+40 14 02.90	13.465	8.579	8.206	8.060	
J20230290+4133466	20 23 02.900	+41 33 46.59	14.780	8.762	8.137	7.809	
J20233816+3938118	20 23 38.161	+39 38 11.84	11.293	8.996	8.829	8.731	
HDE 229258	20 24 25.516	+39 49 28.30	10.235	8.833	8.748	8.689	2
J20252497+3934030	20 25 24.969	+39 34 03.02	15.380	5.209	4.289	3.611	
BD+39 4179	20 25 27.281	+40 24 00.15	11.066	7.210	6.857	6.667	3
J20253116+4005508	20 25 31.164	+40 05 50.82	10.221	6.701	7.153	6.373	
J20253320+4048444	20 25 33.196	+40 48 44.38	13.112	8.340	7.904	7.648	
J20261976+3951425	20 26 19.759	+39 51 42.46	15.600	9.351	8.695	8.348	
J20262484+4001413	20 26 24.841	+40 01 41.25	13.290	9.021	8.571	8.330	
J20272099+4121262	20 27 20.994	+41 21 26.15	13.830	9.448	9.003	8.730	
J20273787+4115468	20 27 37.873	+41 15 46.79	14.570	9.146	8.581	8.263	
J20274925+4017004	20 27 49.251	+40 17 00.42	13.460	8.713	8.315	8.104	
J20275204+4131200	20 27 52.039	+41 31 19.98	10.668	8.769	8.890	8.850	
J20275292+4144067	20 27 52.921	+41 44 06.65	13.330	8.144	7.583	7.277	
J20281176+3840227	20 28 11.757	+38 40 22.73	11.805	8.349	8.077	7.944	
J20285874+4013302	20 28 58.744	+40 13 30.22	15.860	8.494	7.667	7.202	
J20290247+4231159	20 29 02.469	+42 31 15.91	13.330	9.090	8.641	8.426	
BD+40 4193	20 29 13.555	+40 41 03.38	10.412	8.945	8.856	8.812	
J20291617+4057372	20 29 16.173	+40 57 37.19	15.030	8.855	8.241	7.899	
J20293563+4024315	20 29 35.631	+40 24 31.45	12.468	8.831	8.450	8.268	
J20300022+4337553	20 30 00.215	+43 37 55.29	13.326	9.061	8.525	8.323	
J20301097+4120088	20 30 10.970	+41 20 08.82	15.690	9.855	9.202	8.882	
BD+40 4208	20 30 49.972	+40 44 18.53	10.654	8.869	8.739	8.664	
J20314341+4100021	20 31 43.408	+41 00 02.07	15.940	9.885	9.285	8.957	
J20315433+4010067	20 31 54.331	+40 10 06.71	15.990	9.742	9.176	8.884	
J20315898+4107314	20 31 58.983	+41 07 31.41	15.490	9.773	9.164	8.832	
J20315984+4120354	20 31 59.841	+41 20 35.41	10.668	9.119	9.028	8.926	
J20320734+3828586	20 32 07.340	+38 28 58.62	10.440	8.880	8.799	8.726	
CCDM J20323+4152AB	20 32 20.811	+41 52 00.78	9.973	8.694	8.739	8.728	
J20323882+4058469	20 32 38.823	+40 58 46.85	15.430	9.701	9.141	8.821	
J20323968+4050418	20 32 39.682	+40 50 41.83	14.410	9.631	9.156	8.913	
J20330453+3822269	20 33 04.533	+38 22 26.91	11.383	9.021	8.870	8.790	
J20330526+4143367	20 33 05.262	+41 43 36.74	13.940	9.286	8.854	8.624	
BD+41 3801	20 33 30.398	+42 04 17.35	10.507	9.124	9.041	8.967	
LS II +37 97	20 33 35.524	+38 01 36.73	11.838	6.691	6.213	5.900	
J20340430+4136507	20 34 04.297	+41 36 50.67	15.300	9.931	9.234	8.972	
BD+42 3785a	20 34 15.390	+43 09 35.28	10.131	9.009	8.955	8.932	
J20345785+4143543	20 34 57.846	+41 43 54.25	15.430	8.447	7.777	7.417	4
J20361806+4228483	20 36 18.062	+42 28 48.30	15.650	9.814	9.170	8.855	
J20364336+3906145	20 36 43.361	+39 06 14.53	11.530	8.558	8.631	8.565	
J20371773+4156316	20 37 17.734	+41 56 31.57	15.760	9.071	8.367	8.041	
J20381289+4057169	20 38 12.888	+40 57 16.86	12.870	9.183	8.867	8.675	
J20382173+4157069	20 38 21.728	+41 57 06.89	15.810	8.760	8.036	7.682	
J20382889+4009566	20 38 28.889	+40 09 56.63	9.996	8.896	8.841	8.816	
J20395358+4222506	20 39 53.582	+42 22 50.62	15.890	7.345	6.376	5.822	
CCDM J20420+4015	20 42 01.182	+40 14 42.70	9.568	8.688	8.664	8.638	
J20423509+4256364	20 42 35.089	+42 56 36.43	14.480	9.211	8.624	8.304	
CCDM J20429+4311AB	20 42 54.244	+43 10 38.71	8.431	8.515	8.593	8.647	5
J20432737+4308525	20 43 27.370	+43 08 52.47	13.874	8.879	8.293	8.096	
J20440752+4107342	20 44 07.516	+41 07 34.18	15.470	9.562	8.998	8.703	
J20472235+4220523	20 47 22.346	+42 20 52.30	14.950	8.936	8.308	8.085	
J20500396+4300118	20 50 03.964	+43 00 11.76	15.140	8.649	7.944	7.514	
J20504551+421012.6	20 50 45.514	+42 10 12.64	15.050	7.674	6.814	6.440	

Notes. 1 Classified as B5 in the HDE catalog; 2 Classification as B2 in the HDE catalog; 3 Candidate early-type star in Comerón et al. (2008); 4 Classified as early-type star in Comerón et al. (1998) (star B18); 5 Binary.

Table 5. Later-type stars.

Object	α (2000)	δ (USNO B)	B	J (2MASS)	H	K_S	Notes
V438 Cyg	20 18 54.316	+40 03 52.16	12.751	6.939	6.231	5.898	1
J20221467+4030028	20 22 14.671	+40 30 02.78	13.205	6.590	5.948	5.600	2
CCDM J20268 4152AB	20 26 51.134	+41 51 33.42	9.996	7.886	7.675	7.650	3
KZ Cyg	20 27 22.881	+41 04 49.71	13.660	2.927	1.946	1.406	4
J20305152+4048088	20 30 51.518	+40 48 08.83	14.010	4.975	4.078	3.502	5
LHS 3559	20 31 25.661	+38 33 44.24	14.800	9.192	8.627	8.358	6
J20320187+3811599	20 32 01.872	+38 11 59.88	14.620	8.182	7.334	7.009	5
J20322086+3934296	20 32 20.861	+39 34 29.57	12.419	9.353	9.106	8.974	5
J20351367+4055249	20 35 13.670	+40 55 24.92	14.500	9.258	8.650	8.393	5
LTT 16018	20 36 46.031	+38 50 32.72	15.350	9.270	8.707	8.461	6
J20395659+3955267	20 39 56.588	+39 55 26.74	15.520	5.631	4.710	4.112	5
J20421728+4129040	20 42 17.283	+41 29 03.96	12.234	8.858	8.492	8.304	2
V1589 Cyg	20 42 49.148	+41 23 00.16	14.710	9.621	9.003	8.715	7
J20432378+4326017	20 43 23.782	+43 26 01.66	13.390	8.314	7.787	7.461	2
IRC +40446	20 45 14.143	+42 20 06.82	15.890	3.510	2.398	1.731	8
BD+43 3710	20 45 34.726	+43 32 27.26	11.217	6.598	6.143	5.881	9
J20470538+4241065	20 47 05.382	+42 41 06.54	11.577	8.666	8.369	8.216	2
J20481793+4236096	20 48 17.927	+42 36 09.63	12.620	8.620	8.169	7.945	2
BD+41 3896	20 48 36.836	+42 06 26.37	9.965	8.047	7.886	7.784	10
HD 198795	20 51 20.124	+42 37 52.46	10.526	8.482	8.602	8.587	11

Notes. 1) Classical Cepheid (Klagyivik & Szabados 2009); 2) A-type (this work); 3) F5-type close binary (Douglass et al. 2000); 4) M8e Mira variable (Cameron & Nassau 1956); 5) Late type (this work); 6) possible misidentification between USNO-B and 2MASS due to high proper motion; 7) flare star (Pettersen et al. 1988); 8) M8 (Vogt 1973); 9) R:, infrared bipolar nebula (Kraemer et al. 2010); 10) A2 (based on Vilnius photometry); 11) A0 (based on Vilnius photometry).

Table 6. O and B stars from Massey & Thompson (1991) not selected by our criterion.

No. (MT91)	α(2000)	δ(2000)	Sp. type
140	20 31 46.00	+41 17 27.4	O9.5I
258	20 32 27.67	+41 26 21.7	O8V
421	20 33 09.58	+41 13 00.6	O9.5V
425	20 33 10.10	+41 13 10.1	B0V
462	20 33 14.84	+41 18 41.4	O6.5III(f)
465	20 33 15.18	+41 18 50.1	O5.5I(f)
575	20 33 34.36	+41 18 11.6	B1.5V
605	20 33 39.84	+41 22 52.4	B0.5V
736	20 34 09.52	+41 34 13.4	O9V
793	20 34 43.51	+41 29 04.8	B1.5III?

Table 7. Physical parameters of spectroscopically classified O and B stars, assuming $DM = 10.8$.

Object	Sp. type	A_V	T_{eff}	M_V	M ($M_\odot$)	Age (Myr)
		Cygnus OB2				
		Known stars				
BD+40 4179	O8V:	2.2	34877	–3.63	19.8	0.2
BD+40 4185	B0V:	2.4	30110	–4.11	17.7	6.3
HD 195213	O7	3.6	36872	–5.81	43.3	2.8
J20323033+4034332	O9.5IV	6.1	31382	–5.24	26.1	4.9
J20314605+4043246	B0.5IV	4.7	25917	–3.80	14.1	10.0
J20310019+4049497	O7V((f))	4.5	36872	–4.34	25.6	2.0
J20305552+4109575	B0V	5.5	30110	–3.77	16.5	5.6
J20323843+4040445	O8III	6.9	33961	–5.04	28.0	3.9
J20294666+4105083	B0.5V(n) sb2?	4.3	28032	–3.61	14.4	7.9
J20295701+4109538	B0V	4.9	30110	–3.72	16.3	5.6
J20333821+4041064	B0Ia	7.6	25094	–6.60	36.0	4.5
J20313690+4059092	O7Ib(f)	7.7	34990	–5.70	36.0	3.5
J20330292+4047254	O8II((f))	7.0	33570	–6.15	43.9	3.2
J20323498+4052390	B0.2V	5.8	29279	–3.66	15.5	6.3
J20303970+4108489	B0.7Ib	6.2	21514	–6.11	23.0	6.9
J20322734+4055184	B2V	5.1	22608	–4.15	12.1	15.5
V1827 Cyg	Ofpe	8.2	38612	–6.13	57.0	2.2
J20323486+4056174	O8V	6.0	34877	–3.75	20.4	0.8
J20305772+4109575	O9.5V	6.5	31884	–4.16	19.4	4.9
J20345606+4038179	O9.7Iab	6.3	28315	–5.73	29.1	4.9
J20312210+4112029	B2V	5.2	22608	–3.42	11.1	15.5
J20300788+4123504	O8V	7.3	34877	–4.09	21.9	2.2
VI Cyg 3	O9:	5.6	32882	–6.52	53.3	2.8
J20305111+4120218	B0V	6.3	30110	–3.44	15.4	4.5
J20344471+4051465	B0Ia	6.4	25094	–6.48	36.0	4.5
J20344410+4051584	O6.5III(f)	6.9	37134	–4.98	31.3	2.8
J20311833+4121216	O9V	6.3	32882	–4.60	23.0	4.5
J20314540+4118267	O8I	6.0	33179	–5.04	26.0	4.5
J20323154+4114082	O7.5Ib-II(f)	8.0	34084	–5.86	37.0	3.5
J20320689+4117570	B3V	5.5	19262	–3.19	8.6	27.5
J20313338+4122490	B1V	5.5	25953	–3.22	12.3	10.0
J20332346+4109130	O5.5V	7.0	39865	–6.40	68.6	2.0
J20340486+4105129	O9V	5.5	32882	–3.42	17.4	0.8
J20330879+4113179	O4III	6.4	42422	–6.17	62.3	1.5
J20332674+4110595	O8.5V	6.0	33879	–4.14	21.2	3.2
J20331369+4113057	O8V	5.7	34877	–4.00	21.4	2.0
J20325964+4115146	B0V	6.3	30110	–4.19	18.1	6.3
J20331326+4113287	O6V	7.0	38867	–4.43	29.8	1.0
VI Cyg 9	O5If	6.5	38612	–6.82	83.6	2.0
VI Cyg 1	O9V	4.8	32882	–4.81	24.5	4.5
J20340435+4108078	B1V	5.5	25953	–3.26	12.5	10.0
J20340601+4108090	O9.5V	6.5	31884	–4.20	19.6	4.9
J20303980+4136506	O6V	5.9	38867	–4.00	26.3	0.0
VI Cyg 2	B1Ib:	3.2	19979	–4.08	11.3	17.8
J20330292+4117431	O8V	6.2	34877	–4.46	24.0	3.2
J20314965+4128265	O9III	3.8	31846	–3.42	16.7	2.0
J20331748+4117093	O7V	5.4	36872	–4.61	28.1	2.5
LS III +41 30	O9V	4.3	32882	–3.94	19.3	3.5
J20333078+4115226	B1I	6.1	19979	–6.49	25.8	6.3
J20332101+4117401	O9V	4.9	32882	–3.52	17.8	1.4
VI Cyg 4	O7IIIf	4.0	36077	–5.00	30.9	3.2
VI Cyg 8C	O5III	4.7	40307	–5.62	47.6	2.0
VI Cyg 8D	O8.5V	4.8	33879	–3.94	20.3	2.5
J20333700+4116113	B0V	5.4	30110	–4.30	18.7	6.3
J20360451+4056129	O5V((f))	6.4	40862	–4.72	34.8	1.0
VI Cyg 16	O8V(n)	4.0	34877	–4.38	23.5	3.2
VI Cyg 7	O3If	5.0	42233	–5.63	48.3	1.5
J20325002+4123446	O8V	4.7	34877	–4.19	22.5	2.5
VI Cyg 23	O9V	4.8	32882	–3.46	17.6	1.0
VI Cyg 6	O8V	4.4	34877	–4.71	26.0	3.5
V2186 Cyg	B0V	4.7	30110	–3.26	14.9	3.5
J20331803+4121366	O8V	4.9	34877	–4.08	21.9	2.2
J20325919+4124254	O8V	4.6	34877	–3.84	20.8	1.2
LS III +41 32	B0Ib	3.3	25094	–3.10	11.6	11.2

Table 7. continued.

Object	Sp. type	A_V	T_{eff}	M_V	M ($M_\odot$)	Age (Myr)
J20333910+4119258	B0Iab	5.2	25094	–5.59	22.9	6.9
J20335952+4117354	O9.5V	5.0	31884	–4.30	20.1	4.9
J20334783+4120415	B1III	5.2	21353	–4.77	14.1	12.3
J20342193+4117016	O8III + O8III	5.9	33961	–4.70	24.8	3.9
J20334086+4130189	O7V	5.1	36872	–3.61	21.4	0.0
VI Cyg 10	O9.5Ia	5.4	30463	–6.64	49.4	3.2
J20333030+4135578	O8V	6.0	34877	–4.75	26.0	3.5
J20342959+4131455	O7V	6.2	36872	–5.65	41.3	2.8
J20341350+4135027	O7V	4.9	36872	–4.29	25.4	1.8
VI Cyg 11	O5I	5.1	38612	–6.24	59.0	2.2
J20345878+4136174	B0 Ib(n) sb2?	5.7	25094	–5.78	24.7	6.3
		New stars				
J20303833+4010538	B1V	5.7	25953	–3.43	12.5	11.2
J20293473+4020381	B1V	5.2	25953	–3.55	12.8	11.2
J20273982+4040384	B1V	3.0	25953	–3.30	12.5	10.0
J20281539+4044046	B1III	4.1	21353	–4.22	12.1	15.5
BD+40 4210	B1III:e	6.5	21353	–7.66	54.1	3.5
J20310700+4035537	B1III	4.7	21353	–2.98	9.5	20.0
J20292449+4052599	B0.2IV	5.7	27274	–4.14	15.6	8.7
J20303297+4044024	B1V	4.0	25953	–3.36	12.7	10.0
J20282772+4104018	B0.5V	5.2	28032	–3.53	14.2	7.9
J20335842+4019411	O9:	7.3	32882	–5.53	32.0	3.9
J20314885+4038001	B1II	4.4	20666	–2.97	9.1	21.9
J20283039+4105290	OC9.7Ia	6.7	28315	–6.20	34.2	4.5
J20272428+4115458	O9.5V	4.4	31884	–3.29	16.3	1.1
J20301839+4053466	O9V	6.9	32882	–4.45	21.9	4.5
J20284657+4107069	B2II	5.4	17804	–3.00	8.1	31.6
J20321568+4046170	B0.2IV	5.5	27274	–3.34	13.4	7.9
J20294060+4109585	B1[e]	4.5	25953	–3.26	12.5	10.0
J20331130+4042337	B0:III:	6.6	26248	–4.16	15.9	8.7
J20323951+4052475	B0:V:	6.1	30110	–4.31	18.8	6.3
J20293480+4120089	O9.5V	6.9	31884	–3.92	18.4	4.5
BD+40 4223	B0Ia	6.0	25094	–7.00	48.3	3.5
J20333822+4053412	B0Ib	5.5	25094	–4.87	16.9	10.0
J20331870+4059379	B0.5IIIe	7.0	23801	–4.11	13.4	12.3
J20315961+4114505	O7V	5.9	36872	–3.99	23.6	0.6
J20341605+4102196	O9.5V	6.5	31884	–3.84	18.1	3.9
J20354703+4053012	B2V	4.1	22608	–2.95	9.8	17.8
J20331748+4117093	O7V	5.4	36872	–4.61	28.1	2.5
		Cygnus OB9				
		Known stars				
BD+38 4058	B0V	3.2	30110	–4.21	18.2	6.3
HD 228821	B8	–0.1	11800	–2.10	8.2	31.6
HD 228929	B0.5Ib	4.1	22537	–5.60	20.5	7.9
HD 193426	B9Ia	3.5	10500	–6.71	15.4	11.2
HD 229250	O7	3.9	36872	–5.28	33.9	3.2
BD+39 4168	O7	4.6	36872	–5.40	37.3	2.8
HD 228919	B1IV	1.9	23653	–3.54	11.8	14.1
HD 228882	B05Ia	4.0	22537	–5.90	23.0	6.9
HD 228928	B2Ib:nn	2.9	17180	–4.37	10.6	20.0
HD 229202	O8V:	3.0	34877	–4.66	25.0	3.5
HD 228911	B2	0.9	22608	–3.79	11.6	15.5
HD 228941	B3	1.0	19262	–3.39	9.1	25.1
BD+39 4177	O6.5	3.3	37870	–5.51	39.3	2.8
BD+39 4179	B0III	3.4	26248	–3.26	12.5	10.0
HD 194194	B2III	–0.2	18428	–3.07	8.1	31.6
NGC 6910 #14	B0.5V	2.9	28032	–3.77	15.1	7.9
BD+40 4148	O9.5:V	3.4	31884	–4.22	19.7	4.9
BD+40 4146	B3	2.8	19262	–4.31	11.3	17.8
NGC 6910 #16	B3	2.9	19262	–3.56	9.3	25.1
HD 194092	B0.5III	0.5	23801	–3.49	11.7	14.1
BD+40 4159	O9V	3.9	32882	–4.59	22.8	4.5
HD 229196	O5	3.8	40862	–6.19	61.6	2.0
J20240515+4046035	B0.5V	3.8	28032	–3.86	15.4	7.9
HD 193945	B0Vnn	2.2	30110	–5.11	23.8	5.6

Table 7. continued.

Object	Sp. type	A_V	T_{eff}	M_V	M ($M_\odot$)	Age (Myr)
		New stars				
J20221729+3934215	B5Ia	5.8	13400	–4.16	8.2	31.6
J20215115+3937515	B3V	3.1	19262	–3.88	9.9	21.9
J20241767+3920326	B1V	3.5	25953	–3.23	12.3	10.0
J20223944+3935420	B1III	3.1	21353	–3.82	11.1	17.8
J20234624+3937078	B0.7IV	3.2	25011	–3.86	13.7	11.2
J20243872+3930301	B0I:	6.5	25094	–3.97	13.9	11.2
J20183413+4025045	B0.2IV	4.6	27274	–4.52	17.9	7.9
J20215160+3959496	B1Ib	2.9	19979	–2.81	8.5	25.1
J20220879+3958161	B1II	3.8	20666	–3.82	11.1	17.8
J20214410+4012529	B1Ia	6.2	19979	–5.91	20.5	7.9
J20190610+4037004	O9.7Iab	5.1	28315	–4.26	17.0	7.9
J20211677+4023162	B2III	4.8	18428	–3.14	8.1	31.6
J20203933+4031176	B1.5V	4.4	24280	–3.07	10.8	14.1
J20204933+4033027	B1.5V	5.0	24280	–3.25	11.2	14.1
J20194916+4052090	O9.5V	4.8	31884	–4.18	19.4	4.9
J20214868+4043005	B1V	3.1	25953	–3.40	12.9	10.0
J20220454+4042487	B1III	3.3	21353	–3.48	10.1	20.0
J20250591+4020124	B2III	2.6	18428	–2.66	7.8	31.6
J20233375+4045199	B1III	3.4	21353	–2.86	8.9	21.9
J20215593+4110129	B1III	3.3	21353	–2.85	8.9	21.9
J20223777+4140292	O5If	5.2	38612	–5.42	40.1	2.5
		Field				
		Known stars				
BD+38 4098	B9Ib	1.9	10500	–4.38	8.2	31.6
BD+37 3976	B1.5Vn	2.2	24280	–3.30	11.3	14.1
BD+39 4189	B2p?e?	3.8	22608	–5.30	18.6	8.7
LSII+39 53	O7V:	3.6	36872	–4.36	25.6	2.0
HD 196489	B3V	0.5	19262	–3.24	8.6	27.5
HD 194779	B3II	0.4	15541	–4.02	8.7	27.5
HD 194839	B0.5Iae	3.7	22537	–7.11	43.3	3.9
BD+41 3762	B2V	3.3	22608	–3.97	12.0	15.5
J20310838+4202422	O9.7II	5.7	28644	–5.19	22.5	6.3
J20313693+4201218	B0.7Ib	4.8	21514	–5.27	16.9	10.0
BD+41 3794	B0.2III	3.8	25269	–4.87	16.9	10.0
J20342894+4156171	O9V	6.0	32882	–4.11	20.1	3.9
J20314215+4225532	B1Ib	7.5	19979	–7.13	34.2	4.9
LS III +42 17	B1III	3.7	21353	–4.49	13.1	14.1
J20382040+4156563	B0II	7.6	25671	–5.67	24.3	6.3
J20385918+4202395	B0Ib	5.4	25094	–4.19	15.2	10.0
BD+43 3654	O4If	5.1	40422	–6.27	64.6	2.0
BD+42 3835	O9p...	3.4	32882	–5.09	27.0	4.5
HD 199021	B0V	2.0	30110	–4.86	22.7	5.6
		New stars				
J20294195+3859342	B0.2V	4.7	29279	–3.73	15.8	6.3
J20301273+3904216	B1V	4.9	25953	–3.21	12.3	10.0
J20272553+3929246	O9.5V	4.6	31884	–4.23	19.7	4.9
J20313853+4152585	B1.5V	4.6	24280	–3.05	10.8	14.1
J20264025+4233221	B2II	3.3	17804	–2.61	7.8	31.6
BD+42 3760	O8.5V	3.2	33879	–4.28	21.9	3.5
J20312725+4304227	B1.5V	4.8	24280	–3.70	12.7	12.3
J20325571+4307583	O9.5V	4.9	31884	–4.46	21.2	4.9
J20374323+4232334	B1III	5.4	21353	–3.10	9.7	20.0
J20462289+4212311	B3V	4.0	19262	–3.59	9.3	25.1
J20452110+4223514	B2V	5.6	22608	–3.15	10.2	17.8
J20352227+4355305	B0.2IV	5.8	27274	–4.61	18.1	7.9
J20462826+4223417	O9V	5.4	32882	–4.16	20.4	3.9